Suppression of Wnt/β-catenin signaling by EGF receptor is required for hair follicle development

Swamy K. Tripurani[a,†], Yan Wang[a,†], Ying-Xin Fan[a], Massod Rahimi[a], Lily Wong[a], Min-Hyung Lee[a], Matthew F. Starost[b], Jeffrey S. Rubin[c], and Gibbes R. Johnson[a,*]

[a]Division of Biotechnology Review and Research IV, Office of Biotechnology Products, Office of Pharmaceutical Quality, Center for Drug Evaluation and Research, Food and Drug Administration, Silver Spring, MD 20993; [b]Diagnostic and Research Services Branch, Office of the Director, National Institutes of Health, Bethesda, MD 20892; [c]Laboratory of Cellular and Molecular Biology, Center for Cancer Research, National Institutes of Health, Bethesda, MD 20892

ABSTRACT **Mice that lack the epidermal growth factor receptor (EGFR) fail to develop a hair coat, but the mechanism responsible for this deficit is not completely understood. Here, we show that EGFR plays a critical role to attenuate wingless-type MMTV integration site family member (Wnt)/β-catenin signaling during postnatal hair follicle development. Genetic ablation of EGFR in mice resulted in increased mitotic activity in matrix cells, apoptosis in hair follicles, and impaired differentiation of epithelial lineages that form hair. EGFR is activated in wild-type hair follicle stem cells marked with SOX9 or NFATc1 and is essential to restrain proliferation and support stem cell numbers and their quiescence. We observed elevated levels of *Wnt4*, *6*, *7b*, *10a*, *10b*, and *16* transcripts and hyperactivation of the β-catenin pathway in EGFR knockout follicles. Using primary keratinocytes, we linked ligand-induced EGFR activation to suppression of nascent mRNA synthesis of *Wnt* genes. Overexpression of the Wnt antagonist sFRP1 in mice lacking EGFR demonstrated that elevated Wnts are a major cause for the hair follicle defects. Colocalization of transforming growth factor α and Wnts regulated by EGFR in stem cells and progeny indicates that EGFR autocrine loops control Wnts. Our findings define a novel mechanism that integrates EGFR and Wnt/β-catenin pathways to coordinate the delicate balance between proliferation and differentiation during development.**

Monitoring Editor
Mark H. Ginsberg
University of California, San Diego

Received: Aug 6, 2018
Revised: Aug 29, 2018
Accepted: Aug 29, 2018

INTRODUCTION

The epidermal growth factor receptor (EGFR) is the prototypical member of the ERBB family of receptor tyrosine kinases and is activated by ligand-dependent homo- or heterodimerization (Wieduwilt and Moasser, 2008). Several ligands such as EGF, transforming growth factor α (TGF-α), heparin-binding EGF-like growth factor, betacellulin, amphiregulin, epiregulin, and epigen can bind EGFR with varying affinity and stimulate multiple signal transduction pathways (Nanba *et al.*, 2013). EGFR and its ligands are widely expressed in a variety of tissues, and genetic ablation experiments in mice revealed the importance of EGFR and its ligands during embryonic development and in tissue homeostasis during adult life (Nanba *et al.*, 2013). EGFR mutation and/or overexpression can

This article was published online ahead of print in MBoC in Press (http://www.molbiolcell.org/cgi/doi/10.1091/mbc.E18-08-0488) on September 6, 2018.

†These authors contributed equally to this work.

Author contributions: S.K.T. and Y.W. contributed equally to the study; S.K.T., Y.W., and G.R.J. conceived the study; S.K.T. and Y.W. performed most of the experiments with help from Y.-X.F., M.R., L.W., M.-H.L., and M.F.S.; Y.W., S.K.T., Y.-X.F., M.R., M.F.S., J.S.R., and G.R.J. designed the experiments and interpreted and discussed the results; G.R.J. supervised the project; G.R.J. and S.K.T. wrote the manuscript. All authors discussed the results and commented on the manuscript.

No competing interests are declared.

*Address correspondence to: Gibbes R. Johnson (gibbes.johnson@fda.hhs.gov).

Abbreviations used: 4sU, 4-thiouridine; BMP, bone morphogenetic protein; EGFR, epidermal growth factor receptor; GFP, green fluorescent protein; H&E, hematoxylin and eosin; γH2AX, H2A histone family member X phosphorylated on serine 139; ISH, in situ hybridization; KI, kinase-inactive; PBST, phosphate buffer saline–Tween 20; pEGFR, phospho-EGFR; PH3, phospho-histone H3; PPARγ, peroxisome proliferator-activated receptor gamma; qPCR, quantitative real-time PCR; RT, room temperature; sFRP1, secreted frizzled receptor protein 1; Shh, Sonic hedgehog; SWB, Swiss Webster Black; TGFα, transforming growth factor α; Wnt, wingless-type MMTV integration site family member; WT, wild type.

result in aberrant activation, and EGFR is a widely recognized therapeutic target for human cancers of epithelial origin (Scaltriti and Baselga, 2006).

Many studies have shown that hair follicle development is altered in mutants or genetically modified mice related to the EGFR or its ligands (Nanba *et al.*, 2013). Mice lacking EGFR do not produce a hair coat due to arrested hair follicle development (Miettinen *et al.*, 1995; Sibilia and Wagner, 1995; Threadgill *et al.*, 1995; Hansen *et al.*, 1997; Lichtenberger *et al.*, 2013; Mascia *et al.*, 2013). Hair morphogenesis is initiated during embryogenesis with the formation of a placode that undergoes proliferation and differentiation to form hair germ, peg, bulbous peg, and mature hair follicle by postnatal day 7 (P7) in mice (Schmidt-Ullrich and Paus, 2005). At the end of the hair growth phase (anagen), around P14, the hair follicle undergoes regression (catagen) before entering a resting phase (telogen) at P21 (Schneider *et al.*, 2009). After morphogenesis, hair follicles are periodically regenerated throughout adult life. Multiple pulse–chase labeling studies during embryonic hair morphogenesis revealed that hair follicle stem cells first appear within placodes and are marked by expression of the transcription factors SOX9, LHX2, NFATc1, and TCF3, all of which are essential for hair follicle morphogenesis and regeneration (Nowak *et al.*, 2008). Further, many signaling pathways including members from the wingless-type MMTV integration site family member (Wnt), fibroblast growth factor, hedgehog, bone morphogenetic protein (BMP), and Notch families are reported to cross-talk with one another and are essential for hair follicle development (Millar, 2002).

While previous studies demonstrate an important role for EGFR in hair follicle development (Miettinen *et al.*, 1995; Sibilia and Wagner, 1995; Threadgill *et al.*, 1995; Hansen *et al.*, 1997; Lichtenberger *et al.*, 2013; Mascia *et al.*, 2013), the signaling mechanism(s) through which EGFR promotes hair follicle growth is not known. It is similarly unclear whether EGFR is involved in regulating hair follicle stem cell quiescence and proliferation and their maintenance. Here, we show that in the developing hair follicle, β-catenin lies downstream of EGFR signaling, and EGFR performs an essential function to suppress β-catenin activation during morphogenesis. Canonical β-catenin signaling is essential for embryonic hair follicle induction and organogenesis, as well as stem cell activation during telogen to promote entry into the anagen phase of a new hair cycle (Lim and Nusse, 2013). Genetically engineered mouse models reveal that loss of β-catenin in embryonic epidermis prevents hair follicle formation, whereas expression of activated β-catenin results in expansion of hair follicle fate during development and de novo formation of hair follicles in adults (Gat *et al.*, 1998; Huelsken *et al.*, 2001; Lowry *et al.*, 2005; Narhi *et al.*, 2008; Baker *et al.*, 2010; Choi *et al.*, 2013; Lien *et al.*, 2014).

Although EGFR and Wnt/β-catenin signaling have been studied extensively in isolation during mammalian development and disease, antagonism between these two pathways has only been observed in the development of lower organisms such as *Drosophila* and *Caenorhabditis elegans* (Szuts *et al.*, 1997; Yu *et al.*, 2009). In our study, using two different mouse models that lack EGFR kinase activity, we have identified and characterized a new mechanism of antagonism between the pathways that involves the EGFR-mediated suppression of *Wnt* gene expression. This mechanism is required for postnatal hair follicle development, to restrain the proliferation of hair follicle stem cells, and for the maintenance of quiescent stem cell populations. Our findings may have implications for other developmental processes and diseases in which Wnts, β-catenin, and EGFR play critical roles.

RESULTS

Characterization of postnatal skin and hair development in kinase-inactive EGFR knock-in mice

To study the role of EGFR kinase activity in hair morphogenesis, we generated a homozygous EGFR knock-in mouse on a Swiss Webster Black background, in which wild-type (WT) EGFR was replaced with kinase-inactive (KI) EGFR. A single-nucleotide mutation of deoxyadenosine to deoxythymidine (AAG to ATG) within exon 19 of the *Egfr* gene resulted in replacement of an essential lysine residue at position 723 in the kinase domain with methionine (K723M). This conserved lysine in protein kinases forms a salt bridge with a glutamate residue in the αC helix, and is required for ATP binding (Huse and Kuriyan, 2002). A change of lysine at this position to methionine renders the EGFR catalytically inactive, consistent with the crystal structure for this mutant protein (Red Brewer *et al.*, 2009). The homologous recombination targeting event to achieve the mutation is depicted in Supplemental Figure 1A. The neomycin resistance cassette was removed by mating to *EIIa-Cre* mice, and a heterozygous cross-produced mouse that was homozygous for the KI *Egfr* (Supplemental Figure 1B). No embryonic lethality was observed, and >90% of homozygous KI pups survive up to P7, but not beyond P14. As previously reported in other EGFR-null mice models (Sibilia and Wagner, 1995; Threadgill *et al.*, 1995; Hansen *et al.*, 1997), KI pups were born with open eyelids and rudimentary whiskers (Supplemental Figure 1C) and were incapable of producing a coat of hair as they aged (Figure 1A). To assess EGFR protein levels in WT and KI mice, we performed Western blot analyses on skin samples from newborns (P0) and mice at P4 and P7. EGFR protein increased in WT during the first postnatal week and peaked at P7, whereas the EGFR K723M protein was present at lower levels in all ages tested (Supplemental Figure 1D). Murine hair morphogenesis starts around embryonic day 14 and takes place in three waves until just after birth (Duverger and Morasso, 2009). At P0, placode, germ, peg, and bulbous peg structures were all observed in both KI and WT with no histological differences (Supplemental Figure 1E).

To determine whether development of the interfollicular epidermis and the sebaceous gland were affected in KI mice, we investigated the histology and expression of differentiation markers for these skin appendages. No significant histological differences were observed in KI interfollicular epidermis or sebaceous gland compared with WT at P0 or P7. Further, immunofluorescence analyses for markers of the basal (keratin 14), spinous (keratin 1 and 10), and granular (loricrin) layers of the interfollicular epidermis and a marker for sebocytes (peroxisome proliferator-activated receptor gamma [PPARγ]) in sebaceous glands did not reveal any differences between KI and WT in newborn or P7 skin (Supplemental Figure 2, A–D).

While no differences were apparent in early postnatal skin from WT and KI mice, signs of altered hair follicle development were detected as early as P4, and striking histological abnormalities were observed in the hair follicles of KI by P7 (Figure 1B). In general, hair follicle morphogenesis is completed by day 7 in mice (Muller-Rover *et al.*, 2001). Mature hair follicles in WT mice were fully developed at P7 with large hair bulbs that descend deep into the subcutis. In contrast, KI hair follicles at P7 failed to reach the late stages of morphogenesis, did not penetrate fully into the subcutis, were shorter and misoriented, and did not pierce the epidermal surface (Figure 1, B and C). To further characterize the P7 hair follicles, we performed in situ hybridizations (ISHs) to localize transcripts for *Egfr* and its ligand, transforming growth factor α (*Tgfα*). ISH of WT mouse skin detected *Egfr* and *Tgfα* mRNAs in all epithelial compartments of the mature hair follicle with both transcript levels reduced in KI hair follicles (Supplemental Figure 3, A and B). For localization of activated

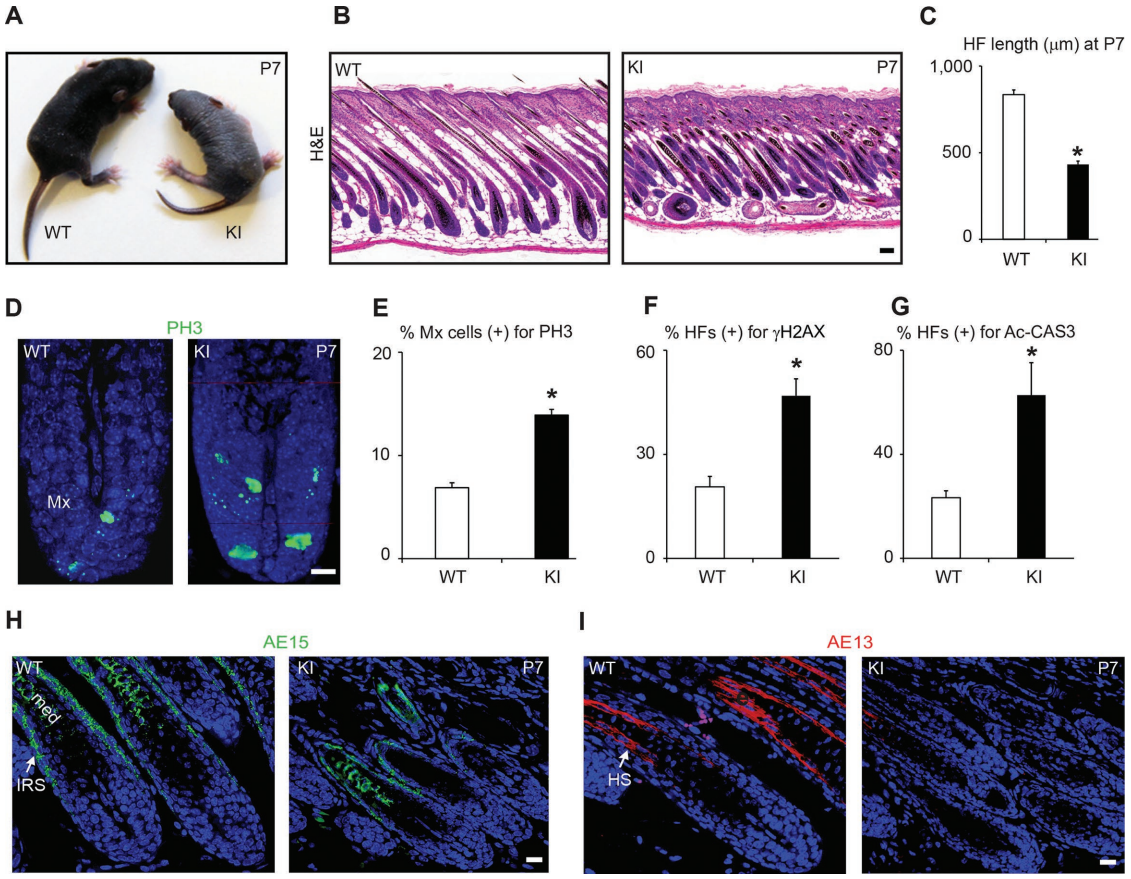

FIGURE 1: Genetic ablation of EGFR kinase increases proliferation, DNA damage, and apoptosis and interferes with differentiation during hair morphogenesis. (A) KI EGFR mice (KI) lack hair coat. (B) H&E-stained KI mouse skin sections reveal aberrant and disoriented hair follicles (HFs). (C) Reduced hair follicle length in KI. (D–I) Immunofluorescence and quantifications. (D, E) Increased mitotic activity (mitosis-specific marker PH3) in KI matrix (Mx) cells. There were 30–75 cells counted per hair follicle. (F, G) Elevated levels of γH2AX (marker of DNA breaks) and activated caspase-3 (Ac-CAS3; apoptosis marker) in KI. (H, I) Reduction of trichohyalin (AE15), an inner root sheath (IRS) and medulla (med) marker, and hair keratin (AE13), a hair shaft (HS) marker of the cortex and medulla in KI. All analyses and pictures were from mice at P7. Graphs contain means with SEM ($n \geq 3$ mice; ≥20 hair follicles/mouse). *p value ≤ 0.05. Scale bars: 10 μm.

EGFR, immunofluorescence microscopy using phospho-EGFR (pEGFR) antibodies was performed at P0, P2, and P7. pEGFR was detected in WT hair follicles at these ages, but was absent from KI hair follicles. Supplemental Figure 3C shows pEGFR staining in the outer root sheath, inner root sheath, matrix, and bulge cells of the WT hair follicle at P7 and lack of any staining in KI follicles. Taken together, these results demonstrate that EGFR kinase activity is necessary for postnatal hair follicle development in mice.

Elevated mitotic activity, DNA damage, apoptosis, and impaired differentiation in KI EGFR hair follicles

As follicles mature during hair morphogenesis, matrix cells proliferate and differentiate to form columns of cells that become the inner root sheath and hair shaft (Alonso and Fuchs, 2006). To understand the mechanism behind the abnormal hair phenotype in KI mice, we next determined whether proliferation and differentiation of matrix cells is affected by loss of EGFR kinase. Immunofluorescence staining for Ki67 (marks proliferating cells during all stages of cell cycle except G0) did not show any differences, as 100% of matrix cells were positive for Ki67 in both WT and KI hair follicles at P7 (unpublished data). To assess variations in matrix proliferation, we stained for phospho-histone H3 (PH3) to identify cells specifically in mitosis, a short and transient event during the cell cycle. Compared with WT, more KI matrix cells were positive for pH3 (Figure 1D), and scoring revealed a ~95% increase in percentage of PH3-positive matrix cells in KI hair follicles at P7 (Figure 1E). In addition to increased mitotic activity in KI matrix cells, we observed degenerating hair follicles in KI mice (Figure 1B). Because uncontrolled proliferation can be associated with a high level of apoptosis (Alenzi, 2004), we next investigated whether DNA damage and apoptosis were increased in KI hair follicles. One of the initial responses to DNA breaks is the phosphorylation of histone H2A at residue Ser-139 (referred to as γH2AX) (Mah *et al.*, 2010). γH2AX localizes and can be detected at sites of double-stranded DNA breaks (Mah *et al.*, 2010), and γH2AX staining is very rarely seen in the murine hair follicle matrix. We found that KI hair follicles positive for γH2AX were significantly increased relative to WT (Figure 1F). Likewise, compared with WT, a higher proportion of hair follicles were positive for activated caspase-3 in KI (Figure 1G). These results demonstrate that loss of EGFR kinase results in aberrant matrix cell proliferation, DNA damage, and apoptosis.

Because KI mice are hairless, we next determined whether differentiation in the cell lineages of the hair shaft and inner root sheath was affected in KI follicles. AE15, which is normally expressed in the inner root sheath and medulla of the hair shaft (O'Guin *et al.*, 1992), was markedly reduced in KI hair follicles (Figure 1H). AE13, a specific

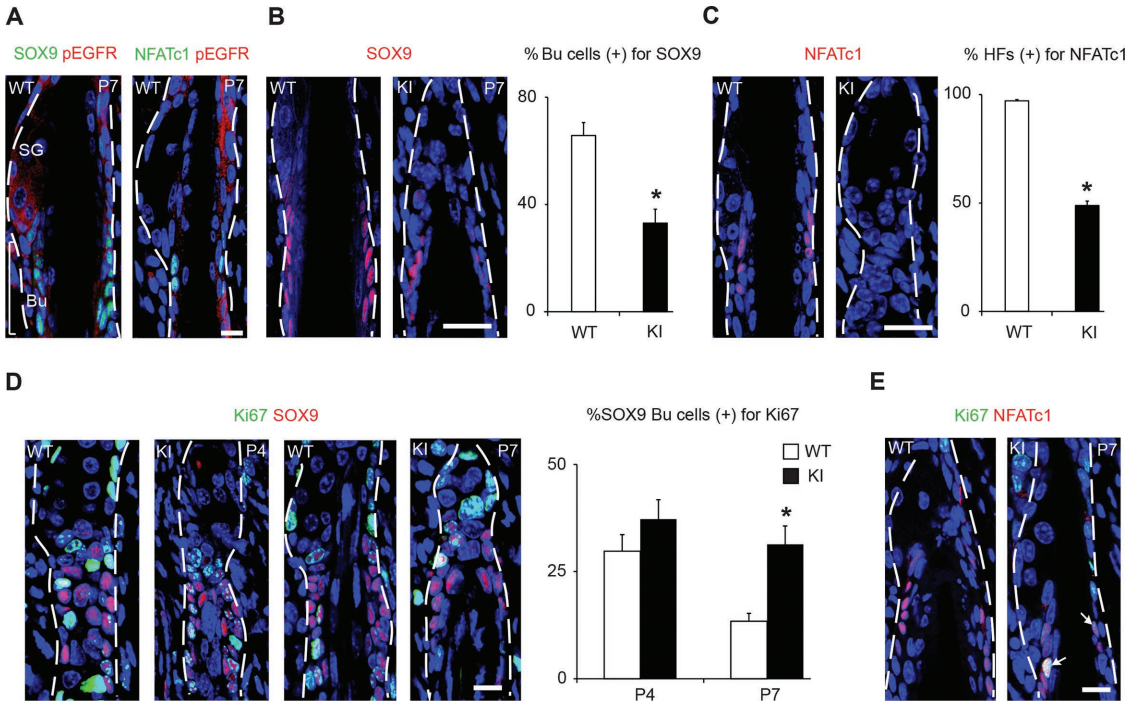

FIGURE 2: EGFR maintains hair follicle stem cell numbers and their quiescence during hair follicle development. (A) Immunofluorescence showing detection of pEGFR in WT bulge (Bu) hair follicle stem cells marked by SOX9 or NFATc1 at P7. (B–E) Immunofluorescence and quantifications. (B) Decreased SOX9 (+) cells in KI bulge. (C) NFATc1 (+) hair follicles are reduced in KI. (D) Increased proliferation of SOX9 (+) cells in KI bulge. (E) Colocalization of NFATc1 and Ki67 in KI (denoted by arrows), but not WT bulge. White dashed line marks the epidermal–dermal boundary. Graphs contain means with SEM ($n \geq 3$ mice; ≥20 hair follicles/mouse). (B, D) There were 30–75 cells counted per hair follicle. *p value ≤ 0.05. Scale bars: 10 μm.

marker for the hair shaft cuticle and cortex keratins (Lynch *et al.*, 1986), was completely absent in KI hair follicles at P7 (Figure 1I). These findings indicate that the absence of visible hair in KI mice results from the inability of matrix cells to differentiate normally and produce the hair shaft and inner root sheath. Our data demonstrate a crucial role for EGFR in regulating matrix cell proliferation and differentiation during hair follicle development.

EGFR is required for maintaining hair follicle stem cell populations and quiescence

Hair follicle stem cell formation and function is dependent on the cells' ability to receive and respond to multiple signaling cues. Inability of hair follicle stem cells to integrate these signals results in abnormal hair follicle development (Blanpain and Fuchs, 2006). We hypothesized that the defects in hair follicle development in KI arose from effects on hair follicle stem cells. To determine whether EGFRs are activated in hair follicle stem cells, we performed double immunofluorescence staining for pEGFR and either SOX9 or NFATc1 in mature WT follicles. As shown in Figure 2A, both SOX9- and NFATc1-expressing cells in the hair follicles of WT bulge were positive for pEGFR. Hair follicle stem cells expressing SOX9 are the earliest stem cells observed in the placode during hair follicle morphogenesis (Nowak *et al.*, 2008). As the embryonic placode develops into a mature hair follicle postnatally, SOX9-positive hair follicle stem cells expand and localize to the bulge in the upper portion of the hair follicle (Vidal *et al.*, 2005; Nowak *et al.*, 2008). Studies have shown that early SOX9-positive hair follicle stem cells fuel the production of transit-amplifying matrix cells required for development of a mature follicle after morphogenesis is initiated (Nowak *et al.*, 2008). SOX9-positive hair follicle stem cells are also essential for the formation of adult bulge hair follicle stem cells populations, which are required for hair morphogenesis and regeneration (Nowak *et al.*, 2008; Kadaja *et al.*, 2014). No differences in SOX9-positive cell numbers between WT and KI were observed in early-stage hair follicles up to P4 (Supplemental Figure 4, A–C); however, while all hair follicles in KI were SOX9-positive at P7, the percentage of bulge cells that were SOX9-positive was half compared with WT (Figure 2B).

NFATc1 is preferentially expressed in quiescent bulge hair follicle stem cells, and in its absence, causes precocious follicular growth (Horsley *et al.*, 2008). NFATc1 was first detected in WT and KI bulbous pegs (Supplemental Figure 4, B–D), but was progressively lost in ~50% of KI follicles by P7 (Figure 2C). Studies have shown that early bulge hair follicle stem cells reduce their cycling rate and become quiescent as the hair follicle develops (Yi, 2017). Quiescent stem cells are characterized by their prolonged presence in the G0 phase of the cell cycle and lack expression of cell proliferation markers such as Ki67 (Cheung and Rando, 2013). Accordingly, we next investigated whether loss of EGFR kinase affects hair follicle stem cell proliferation and quiescence in the bulge, and because cell division is relatively limited in this area of the hair follicle, we used Ki67 to assess proliferation. Ki67 positivity in SOX9-positive bulge cells revealed no differences between WT and KI in early-stage follicles from P0 to P4 (Supplemental Figure 4, E and F), but an increase in the percentage of SOX9-positive bulge cells expressing Ki67 was observed in KI follicles at P7 (Figure 2D). NFATc1-positive hair follicle stem cells in WT follicles did not colabel with Ki67 during morphogenesis as reported previously (Horsley *et al.*, 2008), whereas most hair follicles in KI at P2 through P7 contained NFATc1-positive hair follicle stem cells marked with Ki67 (Supplemental Figure 4, G

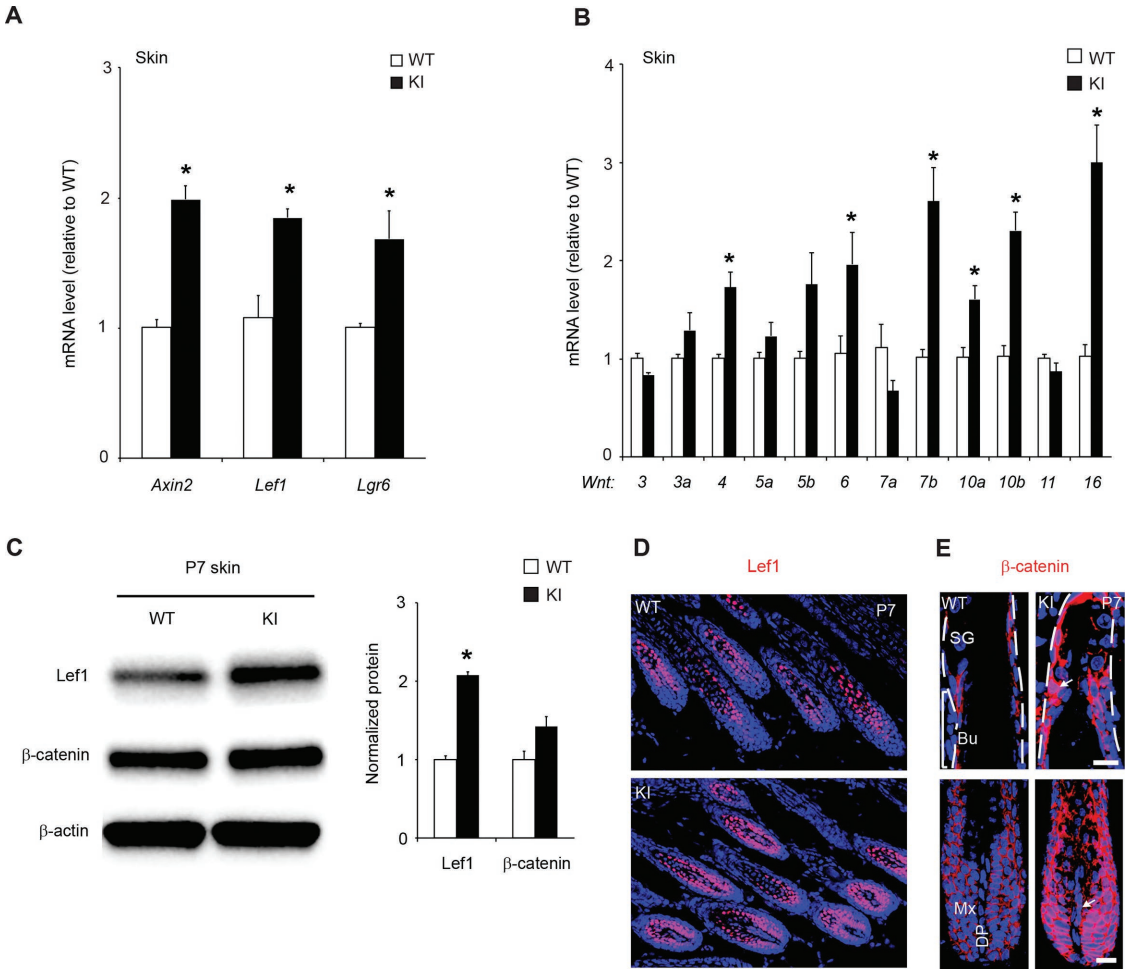

FIGURE 3: Loss of EGFR kinase leads to elevated β-catenin signaling during hair morphogenesis. (A, B) qPCR analysis showing increased transcript levels of Wnt/β-catenin target genes (*Axin2*, *Lef1*, and *Lgr6*) and Wnt ligands (*Wnt4*, *6*, *7b*, *10a*, *10b*, and *16*) in KI skin. Results are presented as relative to WT and are the mean and SEM of five replicates. qPCR transcripts were normalized to the mean of five housekeeping genes *Gapdh*, *B2M*, *Actb*, *GusB*, and *Tbp*. **p* value ≤ 0.05. (C) Western blotting reveals elevated expression of Lef1 and β-catenin protein in KI skin. Bands were quantified by densitometry, and Lef1 and β-catenin intensities were normalized to β-actin and presented relative to WT ($n = 5$). (D) Immunofluorescence showing increased Lef1 protein expression in KI hair follicles. (E) Immunofluorescence showing increased nuclear β-catenin in KI matrix (Mx), dermal papilla (DP), and bulge (Bu) cells (marked by arrows in DP and Bu). All analyses and hair follicle pictures were from mice at P7. Scale bars: 10 μm.

and H, and Figure 2E), demonstrating that quiescence of NFATc1-positive stem cells had been lost in the hair follicles of KI. These findings indicate that EGFR is an important regulator of quiescence, proliferation, and maintenance of hair follicle stem cells during hair development.

β-Catenin signaling is hyperactivated in hair follicles lacking EGFR kinase

Several signaling pathways, such as Wnt/β-catenin, Sonic hedgehog (Shh), Bone morphogenetic protein (BMP), and Notch are known to be involved in hair follicle morphogenesis (Alonso and Fuchs, 2006; Blanpain and Fuchs, 2006). To determine whether these pathways are impacted in KI, we measured target gene expression as an indicator of pathway status using quantitative real-time PCR (qPCR). We found no differences in the expression of target genes associated with BMP (*Id1* and *Id3*), Shh (*Gli1* and *Ptc1*), and Notch (*Hes1* and *Hey1*) pathways (unpublished data). In contrast, transcript levels of Wnt target genes *Axin2*, *Lef1*, and *Lgr6* were elevated in KI skin samples compared with WT (Figure 3A). Extracellular Wnts bind to Frizzled and low-density lipoprotein receptor–related protein 5 and 6 (LRP5/6) receptors to increase nuclear β-catenin and activate target genes (Lim and Nusse, 2013). To test whether EGFR regulates Wnts, we performed qPCR analysis on WT and KI mouse skin sections for *Wnt* transcripts. *Wnt4*, *6*, *7b*, *10a*, *10b*, and *16* transcripts were increased in the KI skin samples compared with WT (Figure 3B). To further characterize the hyperactivation of β-catenin in the skin of KI mice, we measured Lef1 and total β-catenin protein levels by Western blotting. Although total β-catenin protein levels were not significantly different in the skin of WT and KI, Lef1 protein level was approximately twofold higher in KI skin (Figure 3C). We next performed immunofluorescence to examine localization of β-catenin and Lef1 in the hair follicles. Lef1 protein was expressed in the matrix and inner root sheath of WT follicles, and its expression was elevated in KI hair follicles (Figure 3D). Compared with WT, increased nuclear accumulation of β-catenin was observed in KI matrix, dermal papilla, and Wnt/β-catenin signaling (Figure 3E). These results demonstrate that the Wnt/β-catenin pathway is activated upon loss of EGFR kinase activity in skin.

Wnt4, 6, 7b, 10a, 10b, and *16* transcripts are increased in KI EGFR mouse hair follicles

Wnts are highly conserved, cysteine-rich secreted glycoproteins that can act locally on neighboring cells or on the Wnt-secreting cells themselves, and 19 Wnts have been identified in mice and humans (Mikels and Nusse, 2006). Many Wnts are expressed within developing skin and the hair follicle and are essential for hair morphogenesis, hair cycling, and hair follicle stem cell homeostasis (Reddy *et al.*, 2001; Castilho *et al.*, 2009; Fu and Hsu, 2013; Li *et al.*, 2013; Myung *et al.*, 2013; Kandyba and Kobielak, 2014; Zhu *et al.*, 2014). To identify the cellular sources of elevated Wnt production in KI follicles, we performed chromogenic ISHs for *Wnts* that were increased in our qPCR analyses. Compared with WT, *Wnt4 and Wnt6* mRNAs were increased in bulge, outer root sheath, matrix, and dermal papilla, *Wnt7b* was elevated in bulge, *Wnt10a* and *Wnt10b* were elevated in the inner root sheath and matrix, and *Wnt16* expression was high in matrix and bulge of KI follicles (Figure 4). These findings demonstrate that EGFR kinase activity controls *Wnt* mRNA levels within hair follicles.

Elevated Wnt/β-catenin signaling in hair follicle stem cells lacking EGFR kinase

Multiple gain- and loss-of-function studies demonstrated that Wnt/β-catenin is required for maintenance and quiescence of the hair follicle stem cells (Gat *et al.*, 1998; Huelsken *et al.*, 2001; Lowry *et al.*, 2005;

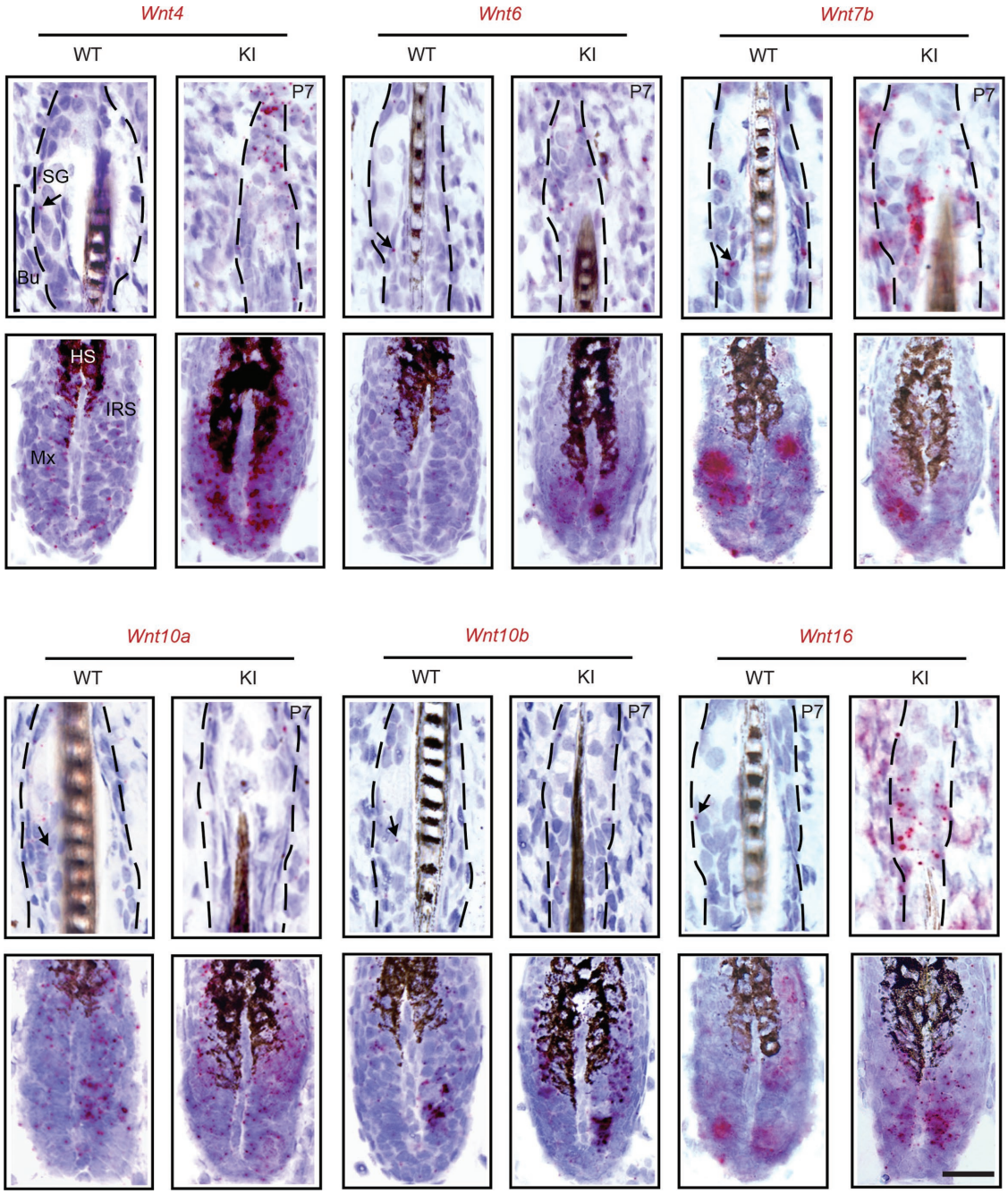

FIGURE 4: Multiple *Wnt* transcripts were elevated in KI EGFR hair follicles. Chromogenic ISHs reveal increased *Wnt4*, *Wnt6*, and *Wnt16* mRNAs (red spots) in KI matrix (Mx) and bulge (Bu), *Wnt7b* in KI bulge, and *Wnt10a* and *Wnt10b* mRNA in KI inner root sheath (IRS) and matrix. Arrows in WT denote in situ staining in bulge. All hair follicle pictures were from mice at P7. Scale bars: 10 μm.

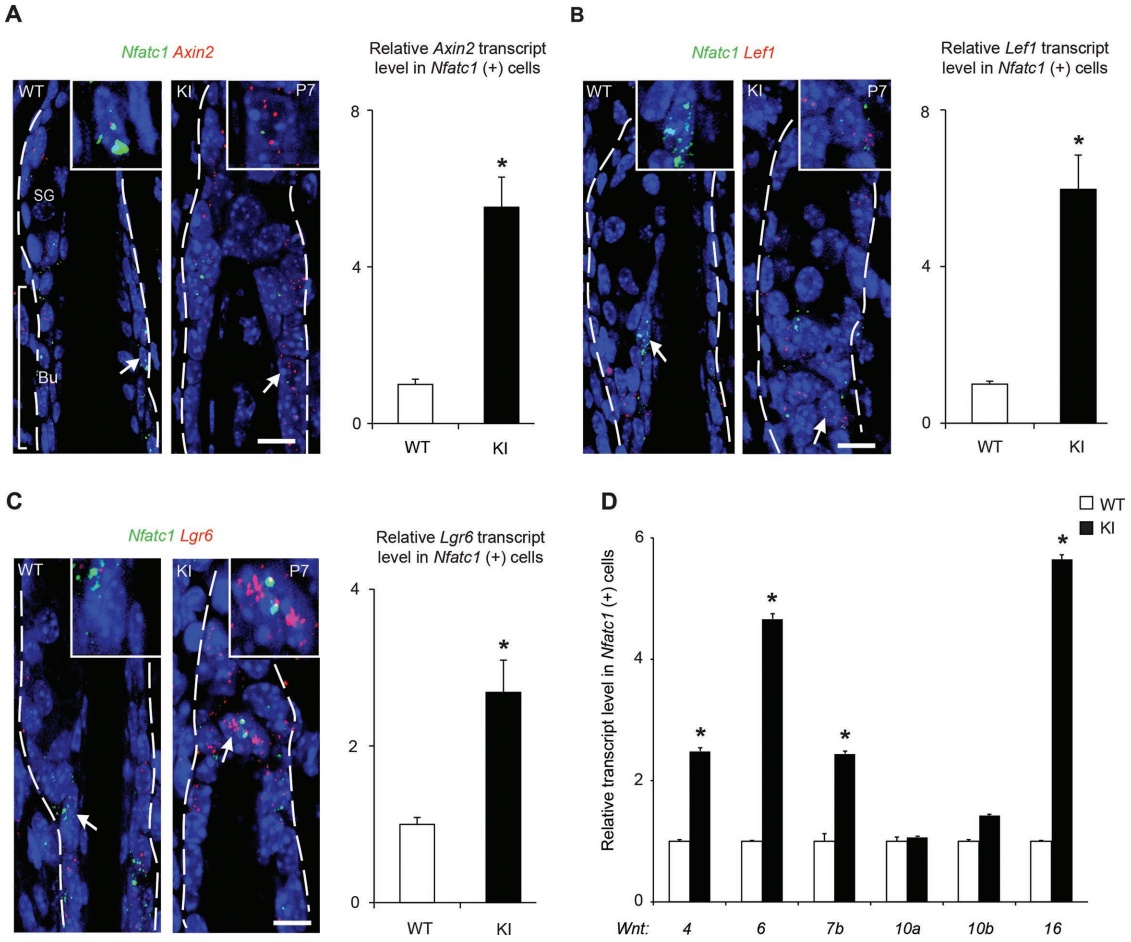

FIGURE 5: EGFR regulates Wnt/β-catenin signaling in hair follicle stem cells. (A–C) Multiplex fluorescence ISHs and quantifications showing increased transcript expression of Wnt/β-catenin target genes *Axin2*, *Lef1*, and *Lgr6* in *Nfatc1* (+) cells in KI bulge. A representative ISH image is shown to the left of the bar graph. Arrows in A–C denote a nucleus magnified in the inset. (D) Quantifications of multiplex fluorescence ISHs demonstrate elevated *Wnt4*, *6*, *7b*, and *16* transcript levels in *Nfatc1* (+) cells in KI bulge. All analyses and hair follicle pictures were from mice at P7. Graphs contain means with SEM ($n \geq 3$ mice; ≥20 hair follicles/mouse; 25–50 cells counted per hair follicle). KI values are relative to WT (set to 1). *p value ≤ 0.05. Scale bars: 10 μm.

Narhi *et al.*, 2008; Baker *et al.*, 2010; Choi *et al.*, 2013; Lien *et al.*, 2014). To quantify mRNA levels of Wnts and their target genes in bulge hair follicle stem cells, we performed RNAscope multiplex fluorescence ISH. RNAscope multiplex fluorescence ISH technique uses a unique probe design strategy that allows detection and quantification of up to four genes in complex tissues with high sensitivity and specificity. Each individual target RNA molecule appears as a distinct punctate dot that can be quantified (Wang *et al.*, 2012). To score Wnts and target gene (*Axin2*, *Lef1*, and *Lgr6*) mRNA levels, we first identified cells positive for *Nfatc1* in the bulge, and the transcript levels were determined by manually counting the number of signal dots in these cells. These analyses revealed increased amounts of all three Wnt target gene transcripts in *Nfatc1*-positive stem cells in the hair follicles of KI relative to WT (Figure 5, A–C). Likewise, *Axin2* transcripts were up-regulated when measured in *Sox9*-positive stem cells in the bulge of KI (Supplemental Figure 5A). With the exception of Wnt*10a* and *10b*, we found that *Wnt4*, *6*, *7b*, and *16* mRNAs were more abundant in KI EGFR hair follicle stem cells compared with WT (Figure 5D). *Wnt4* and *7b* analyses in *Sox9*-positive stem cells in the bulge produced similar results (Supplemental Figure 5, B and C). These findings demonstrate that EGFR kinase activity controls *Wnts* and β-catenin signaling in hair follicle stem cells.

Ligand-induced EGFR activation suppresses *Wnt* gene transcription

Because loss of EGFR kinase activity in mice resulted in the elevation of multiple *Wnt* transcripts in hair follicle, we hypothesized that growth factor–stimulated activation of the EGFR would rapidly decrease *Wnt* mRNA levels in cells. To test this mechanism, we isolated primary keratinocytes from WT mouse skin, treated the cells with TGFα for 6 h, and measured *Wnt* transcript levels using qPCR. Relative to control, TGFα stimulation decreased mRNAs for *Wnt4*, *6*, *7b*, *10a*, *10b*, and *16* in the keratinocytes (Figure 6A). As EGFR activation leads to a rapid decrease in cellular *Wnt* transcript levels, we hypothesized that these changes were due to reductions in gene transcription rates. To test this hypothesis, we used metabolic labeling of newly synthesized RNA with 4-thiouridine (4sU), because 4sU-labeling allows for the separation of newly synthesized RNA from the pre-existing RNA, providing an opportunity to measure RNA transcription rates in real time (Radle *et al.*, 2013). Primary mouse keratinocyte cultures were preincubated with 4sU and then treated with or without TGFα. Total RNA was extracted, followed by thiol-specific biotinylation of 4sU-labeled newly synthesized RNA and purification using streptavidin-coated magnetic beads. qPCR analysis of newly transcribed RNAs revealed that growth factor–induced

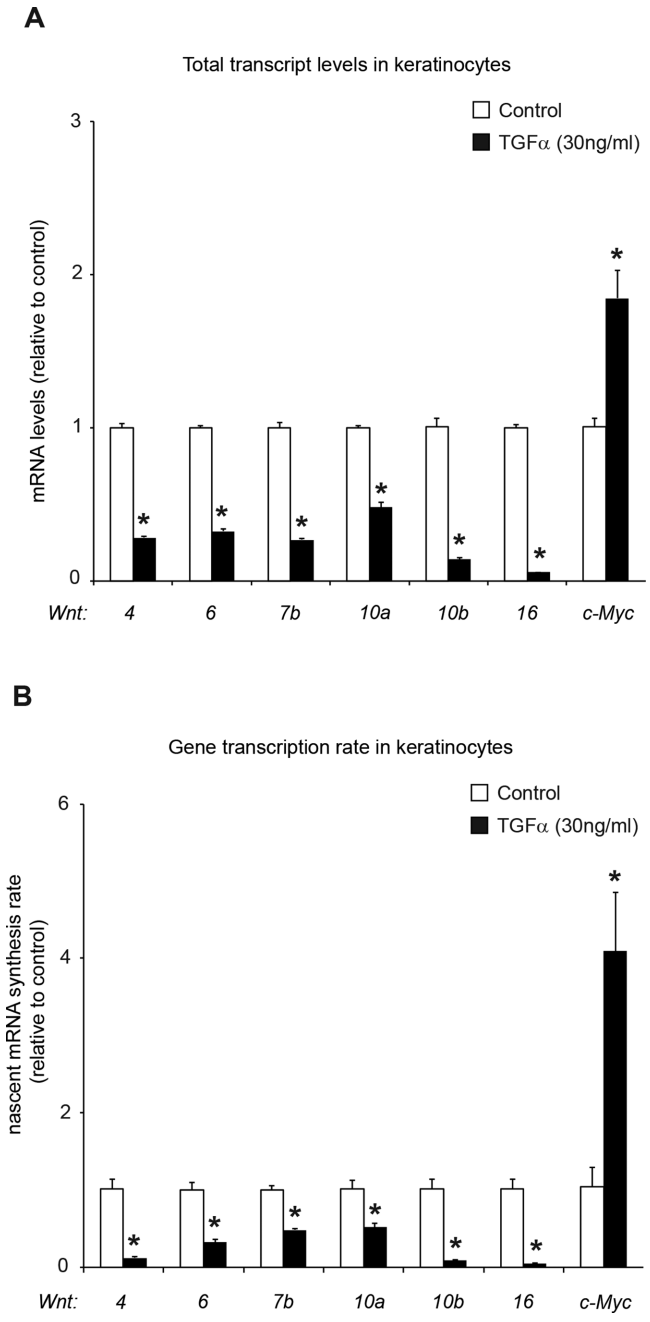

FIGURE 6: Ligand-induced EGFR activation suppresses nascent Wnt mRNA synthesis. (A) qPCR measurements of *Wnt* mRNAs in primary mouse keratinocytes isolated from P0 WT skin and treated without (control) or with TGFα (30 ng/ml) for 6 h. The levels of *Wnt4*, *6*, *7b*, *10a*, *10b*, and *16* mRNA were decreased by TGFα in primary mouse keratinocytes. (B) qPCR measurements of 4sU-labeled, newly transcribed *Wnt* mRNAs isolated from primary mouse keratinocytes treated without (control) or with TGFα (30 ng/ml) for 3 h. *c-Myc* mRNA levels were measured as positive control for TGFα treatment. Results are presented as relative to control and are the mean and SEM of three replicates. qPCR transcripts were normalized to the housekeeping genes *Gapdh* and *B2m*. **p* value ≤ 0.05.

EGFR activation decreased the transcription rates of *Wnt4*, *6*, *7b*, *10a*, *10b*, and *16* within 3 h upon TGFα stimulation (Figure 6B). As expected, cellular *c-Myc* transcript levels and nascent mRNA levels were increased upon TGFα treatment (Figure 6, A and B). These results demonstrate that ligand-stimulated activation of the EGFR decreases the transcription rate of *Wnt* genes.

Negative regulation of *Wnts* by EGFR is mediated by Ras

Ligand-induced stimulation of EGFR leads to downstream activation of Ras and cytoplasmic signaling cascades, which are among the best characterized effector pathways in mammalian skin (Kern *et al.*, 2011). To determine whether EGFR signaling through Ras is involved in the negative regulation of *Wnt* transcripts, we prepared cultures of primary mouse keratinocytes. These cultures were then transduced with either doxycycline-inducible WT Ras or dominant-negative Ras (S17N Ras), and treated with or without EGF. Western blot analyses confirming expression of Ras and the activation status of extracellular signal–regulated kinase (ERK) are shown in Supplemental Figure 6A. Expression of WT Ras alone, but not S17N Ras, mimicked EGF and reduced transcript levels of *Wnt4*, *6*, *7b*, *10b*, and *16* relative to uninduced cells. Conversely, expression of S17N Ras abrogated the EGF-induced decrease in *Wnt4*, *6*, *7b*, *10a*, *10b*, and *16* mRNA levels (Supplemental Figure 6, B–G). Taken together, these results provide a mechanism whereby EGFR signals from the plasma membrane to the nucleus via Ras to control *Wnt* mRNA levels in keratinocytes.

Elevated Wnt signaling is a major cause for the hair follicle abnormalities in mice that lack EGFR kinase

To determine whether the elevated Wnts in KI mice contributed to the abnormal hair follicle phenotype, we used an adenovirus that expresses the Wnt antagonist secreted frizzled receptor protein 1 (sFRP1). sFRP1 inhibits Wnt signaling by interfering with Wnt binding to frizzled receptors (Uren *et al.*, 2000). In these experiments 4-d-old KI mice received a single dorsal subcutaneous injection of adenovirus expressing either sFRP1 or control green fluorescent protein (GFP), and skin sections were harvested and analyzed at P7. Western blot analyses of sFRP1 in skin samples from KI mice that were administered sFRP1 adenovirus confirmed expression of sFRP1 protein (Figure 7B). As expected, sFRP1 expression resulted in a reduction in nuclear β-catenin localization in matrix, dermal papilla, and bulge cells relative to KI mice administered GFP adenovirus (Figure 7C). Although no hair shafts erupted through the skin surface, histological examination of hematoxylin and eosin (H&E) back skin sections and measurement of hair follicle lengths revealed that adenovirus-mediated expression of sFRP1 specifically altered the shape of the KI follicles, producing a morphology more like that of WT follicles (Figure 7, A and D). For determination of whether sFRP1 adenovirus could rescue the impaired matrix cell differentiation in the hair follicles of KI, immunofluorescence analysis of AE13 was performed. Detection of AE13 within the hair shaft of follicles from KI mice was increased by sFRP1 adenovirus when compared with the GFP adenovirus control (Figure 7E), demonstrating that cytodifferentiation was partially restored. sFRP1 adenovirus also mitigated the increased mitotic activity, DNA breaks, and apoptosis observed in KI follicles (Figure 7, F–H).

Because loss of EGFR kinase causes increased β-catenin signaling in hair follicle stem cells and impacts their proliferation and quiescence, we assessed β-catenin target genes, proliferation, and stem cell populations in mice treated with the adenoviruses. In *Sox9*- and *Nfatc1*-positive bulge cells, *Axin2* expression was specifically decreased to WT levels in KI skin treated with sFRP1 adenovirus (Figure 7, I and J). sFRP1 administration restored the presence of SOX9-positive bulge cells and NFATc1-positive hair follicles in KI mice (Figure 7, K and L). Further, sFRP1 expression decreased proliferation in SOX9-positive bulge cells in KI follicles to normal WT

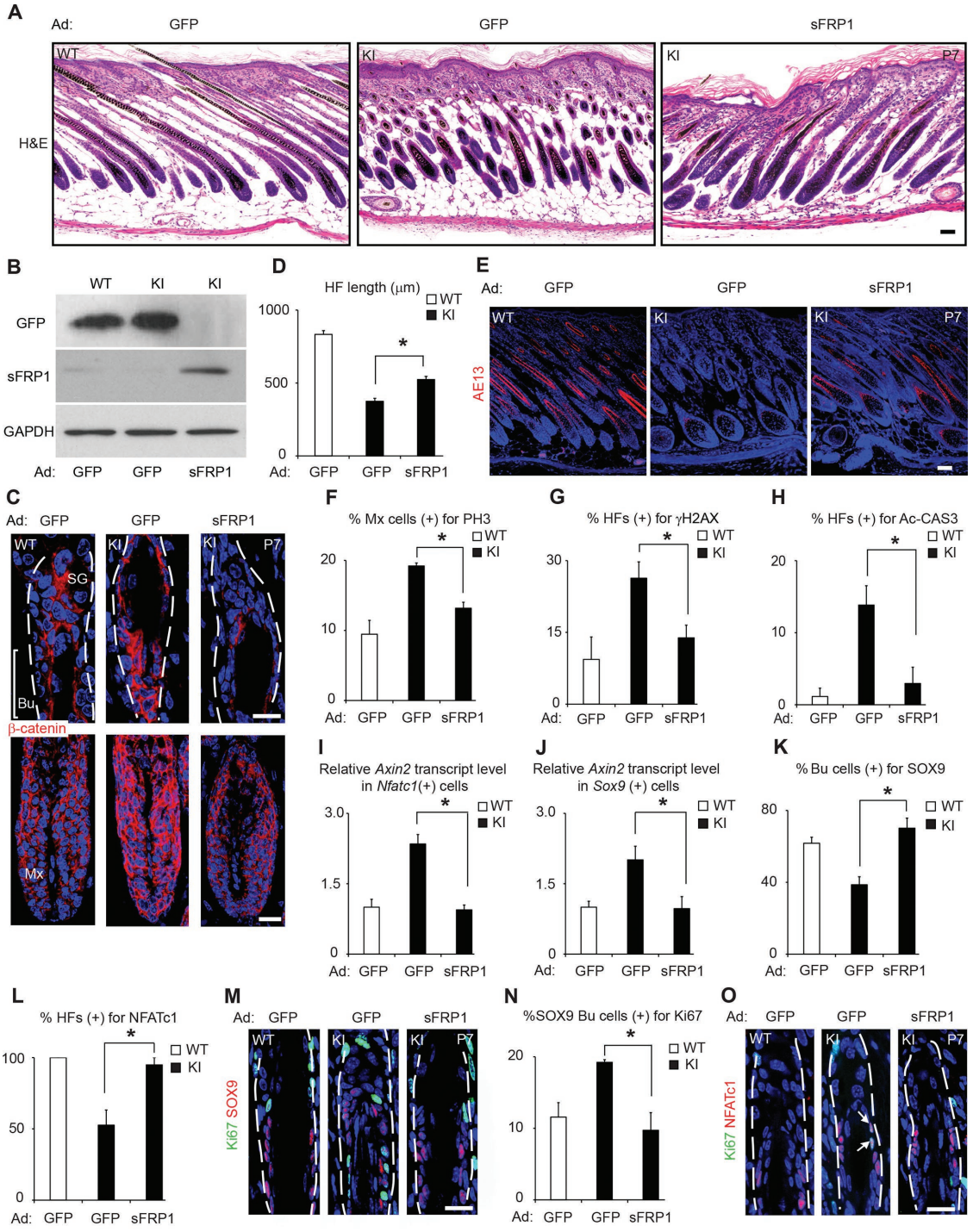

FIGURE 7: Overexpression of the Wnt antagonist sFRP1 rescues hair follicle defects in mice lacking EGFR. (A) H&E sections from KI mice injected with adenovirus (Ad) expressing sFRP1 compared with KI mice injected with adenovirus expressing GFP reveal partial rescue of hair follicle morphology. (B) Western blotting confirms expression of sFRP1 by adenovirus in skin. (C) sFRP1 expression reduces nuclear β-catenin in KI matrix (Mx) and bulge (Bu) cells. (D) Hair follicle length increase in KI treated with sFRP1 adenovirus. (E–O) Immunofluorescence and quantifications. (E) sFRP1 restores hair keratin (AE13) in KI follicles. (F) Decreased mitotic activity (mitosis-specific marker phospho-histone H3, PH3) in KI matrix cells by sFRP1-expressing adenovirus. (G, H) γH2AX (+) and activated caspase-3 (+) (Ac-CAS3) hair follicles are reduced in KI treated with sFRP1 adenovirus. (I, J) sFRP1 expression decreases *Axin2* transcripts in *Nfatc1* (+) and *Sox9* (+) stem cells in KI. (K, L) SOX9 (+) cells in the bulge and NFATc1 (+) hair follicles are rescued by sFRP1 in KI. (M, N) Adenovirus expressing sFRP1 reduces proliferation of SOX9 (+) cells in KI bulge. (O) sFRP1 restores quiescence of NFATc1 (+) cells in KI. Arrows denote NFATc1/Ki67 double-positive cells in KI treated with GFP adenovirus. Mice were treated with adenovirus at P4, and analyses were performed at P7. Graphs contain means with SEM ($n \geq 3$ mice; ≥20 hair follicles/mouse). (F, I–K, N) There were 50–150 cells counted per hair follicle. KI values are relative to WT (set to 1). *p value ≤ 0.05. Scale bars: 10 μm.

levels, as demonstrated by Ki67 staining (Figure 7, M and N). As in WT, no NFATc1/Ki67 double-positive cells were detected in KI skin injected with sFRP1 adenovirus (Figure 7O), demonstrating that quiescence was rescued in EGFR kinase-null NFATc1-positive cells. Taken together, these data provide compelling evidence that the overexpression of Wnts is largely responsible for the hair follicle phenotype observed in mice that lack EGFR kinase activity.

Skin-targeted deletion of EGFR produces a hair follicle phenotype identical to that observed in KI EGFR mice

Because previous studies established that developmental phenotypes associated with reduced or ablated EGFR activity can be influenced by genetic background (Sibilia and Wagner, 1995; Threadgill *et al.*, 1995), we generated a skin-targeted deletion of EGFR using keratin 14 (K14) promoter driven–Cre recombinase (*Egfr* $^{flox/flox}$*K-14cre*) (Vasioukhin *et al.*, 1999; Dassule *et al.*, 2000) in a C57BL/6N background. *Egfr* $^{flox/flox}$ *K14cre* mice did not produce a hair coat, and the majority did not live beyond P21 (Figure 8A). The few mice that survived beyond 3 wk progressively developed a skin rash phenotype that was very similar to that observed in mice with skin-targeted deletion of EGFR using keratin 5 (K5) promoter driven–Cre recombinase (Lichtenberger *et al.*, 2013; Mascia *et al.*, 2013). Like KI mice, *Egfr* $^{flox/flox}$*K14cre* mice displayed aberrant hair follicle morphology, defective hair shaft differentiation, increased proliferation, and DNA breaks and apoptosis in the hair follicle matrix compared with the *Egfr* $^{flox/flox}$ controls (Figure 8, B–F). K14-Cre–mediated deletion of EGFR resulted in loss of SOX9-positive and NFATc1-positive hair follicle stem cells, increased proliferation of SOX9-positive cells, and loss of quiescence in the NFATc1-positive population (Figure 8, G–J). As expected, elevated levels of nuclear β-catenin and *Wnt4* transcripts were detected in matrix, dermal papilla, and bulge, and *Wnt10b* mRNA was higher in the matrix of EGFR-null hair follicles (Figure 8, K–M). These results demonstrate that skin-targeted deletion of EGFR recapitulates the hair follicle and Wnt/β-catenin signaling abnormalities found in KI mice and that the observed phenotype is independent of mouse strain.

TGFα and Wnts controlled by EGFR are coexpressed in hair follicle stem cells and their progeny

In addition to TGFα, transcripts for the other six EGFR ligands (*Areg*, *Btc*, *Egf*, *Epgn*, *Ereg*, and *Hbegf*) were found to be present in various compartments of WT follicles (Supplemental Figure 7). This abundant expression of EGFR ligands and the pervasive EGFR activation in the developing hair follicle implied EGFR autocrine signaling during hair morphogenesis. To further support the concept that autocrine EGFR loops suppress *Wnt* transcripts and signaling, we performed multiplex fluorescence ISH to simultaneously detect EGFR-regulated *Wnt* and EGFR ligand transcripts in WT follicular cells. We found *Tgfα* transcripts colocalized with *Wnt4*, *7b*, and *16* in hair follicle stem cells marked by *Nfatc1* (Figure 9, A–C). Similarly, *Tgfα* transcripts were colocalized with *Wnt4* in matrix (Figure 9D) and *Wnt10b* in inner root sheath cells (Figure 9E), and *Areg* transcripts were colocalized with *Wnt4* in outer root sheath cells (Figure 9F). Thus, in hair follicle stem cells, EGFR acts to suppress Wnts, but these cells are also simultaneously expressing activators of the EGFR. This was also observed in cells of the outer root sheath cells, inner root sheath, and matrix.

DISCUSSION

Studies from the 1990s demonstrated that knockout of EGFR in mice severely impacts development of many tissues and organs, including hair, lung, gastrointestinal tract, kidney, and liver (Miettinen *et al.*, 1995; Sibilia and Wagner, 1995; Threadgill *et al.*, 1995), but the underlying mechanisms responsible for these defects remain elusive. Using two different mouse models that lack EGFR kinase (KI EGFR knock-in and skin-targeted EGFR knockout), we studied the mechanism responsible for the developmental defects observed in hair follicles. Consistent with previous studies (Sibilia and Wagner, 1995; Hansen *et al.*, 1997; Bichsel *et al.*, 2016), we found that loss of EGFR kinase did not alter early hair follicle morphogenesis, but had a profound effect on follicle development postnatally. An important clue came from our unexpected finding that the transit-amplifying matrix cells in the KI mice were dividing at an abnormally high rate. Because these mice lacked a receptor kinase activity associated with growth, this finding seemed paradoxical. However, the identification of increased nuclear accumulation of β-catenin (indicative of hyperactive Wnt signaling) in hair follicles lacking EGFR crystallized the idea that β-catenin activity is controlled by the EGFR during hair development. Genetically engineered mouse models revealed that loss of β-catenin in embryonic epidermis prevents hair follicle formation, whereas expression of activated β-catenin results in aberrant hair morphogenesis in embryos and de novo hair follicle formation and hair tumors in adults (Gat *et al.*, 1998; Lo Celso *et al.*, 2004; Narhi *et al.*, 2008). It has been proposed that β-catenin activation in follicular keratinocytes is critical to the proper balance of proliferation and differentiation of matrix cells, and mounting evidence indicates that quantitative differences in the level of β-catenin signaling influence the choice of lineage adopted by follicular cells during anagen (Baker *et al.*, 2010; Choi *et al.*, 2013). We found that activated EGFR exists in all epithelial compartments of the hair follicle in WT. In KI follicles, we detected elevated *Wnt* transcripts and nuclear β-catenin in the same compartments, which provided a strong connection between loss of EGFR and up-regulation of *Wnts* in vivo. Further, using adenovirus that expressed the Wnt antagonist SFRP1, we demonstrated that the aberrant overexpression of Wnts was a major cause of the abnormal hair follicle phenotype in mice lacking EGFR kinase activity. By interfering with the exaggerated Wnt/β-catenin signaling in the hair follicles of KI, we partially restored the normal balance between proliferation and differentiation in the developing postnatal hair follicle. The partial restoration of hair follicle length and AE13 expression in KI mice administered with sFRP1 adenovirus indicates that, in addition to EGFR's role in suppressing β-catenin signaling, other mechanisms must also be required to complete hair morphogenesis. In summary, our study reveals an important role of EGFR in multiple processes integral to hair follicle development, particularly as a critical regulator of *Wnt* expression and β-catenin activity.

Hair morphogenesis and regeneration are reported to be driven by the same key signaling pathways (Sennett and Rendl, 2012). Loss- and gain-of-function studies established a role for Wnt/β-catenin signaling as an anagen inducer (Lim and Nusse, 2013). Wnt/β-catenin signaling markedly increases during anagen and subsequently decreases as the hair follicle enters catagen and telogen (Choi *et al.*, 2013; Kandyba *et al.*, 2013; Lim *et al.*, 2016). This transition is important for catagen induction, including quiescence and maintenance of hair follicle stem cells in telogen (Choi *et al.*, 2013; Kandyba *et al.*, 2013). Wnt/β-catenin activation, in combination with BMP inhibition, facilitates the transition of hair follicles from telogen to anagen (Kandyba *et al.*, 2013); however, the signals controlling the anagen to catagen transition remain largely unknown. Previous studies have demonstrated increased EGFR activation at the initiation of catagen, and EGFR-null hair follicles do not enter catagen (Bichsel *et al.*, 2016). We believe that EGFR is required for anagen to catagen transition by inhibiting *Wnt* expression and β-catenin activity in hair follicles before the onset of catagen.

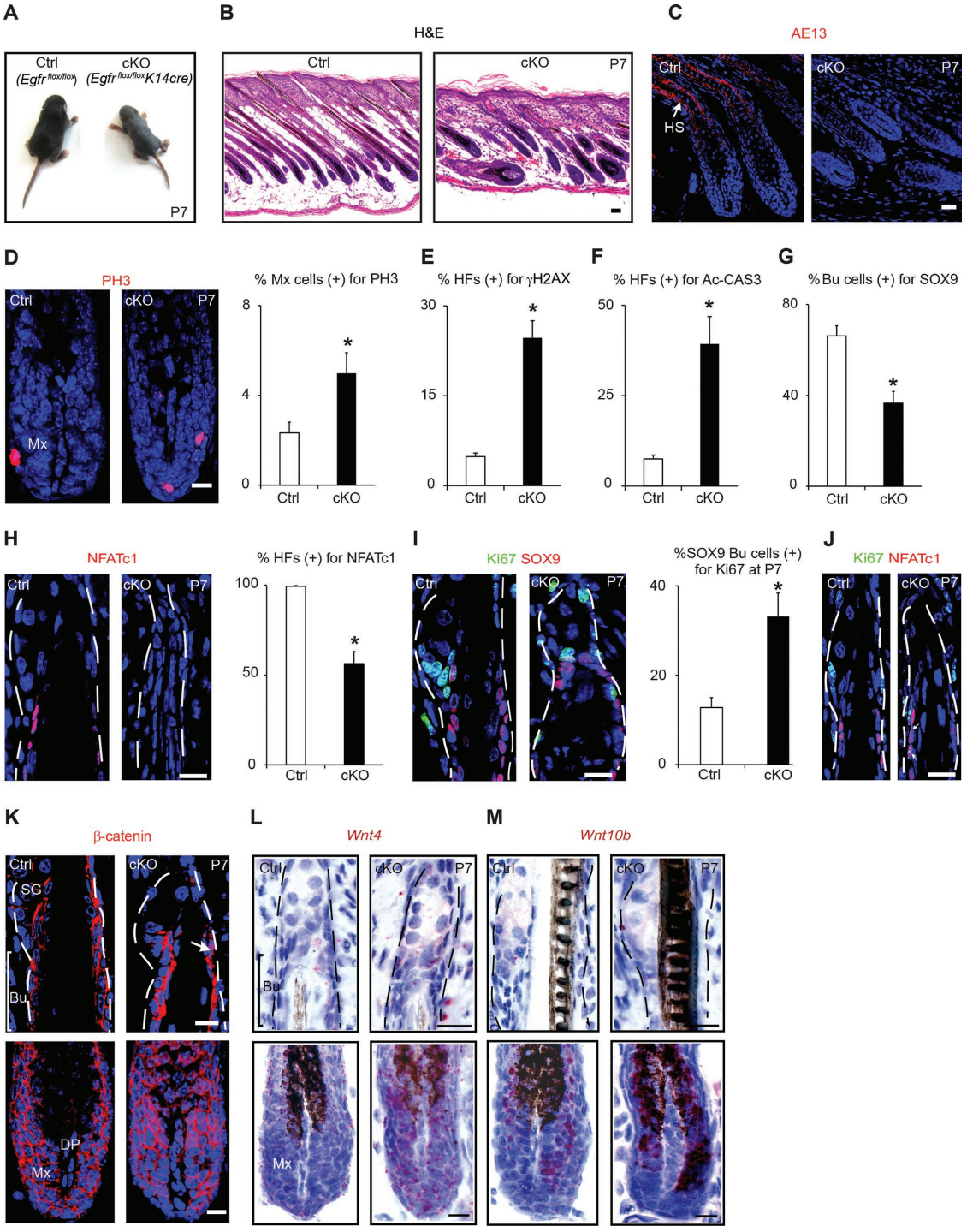

FIGURE 8: Conditional deletion of EGFR in skin results in hair follicle abnormalities identical to KI mice. (A) Mice with skin-targeted deletion of EGFR (*Egfr*$^{flox/flox}$*K14cre*) fail to produce hair coat. (B) H&E-stained P7 skin sections from *Egfr*$^{flox/flox}$*K14cre* mice demonstrate abnormal and misaligned hair follicles. (C) Loss of hair keratin (AE13), a hair shaft (HS) differentiation marker of the cortex and medulla in *Egfr*$^{flox/flox}$*K14cre* mice. (D) Immunofluorescence and quantification of mitosis-specific marker phospho-histone H3 (PH3) showing increased mitotic activity in matrix (Mx) cells of *Egfr*$^{flox/flox}$*K14cre*. (E, F) Elevated levels of γH2AX (marker of DNA breaks) and activated caspase-3 (Ac-CAS3; apoptosis marker) in *Egfr*$^{flox/flox}$*K14cre* follicles. (G) Immunofluorescence and quantification of hair follicle stem cells marked by SOX9 showing reduced SOX9 (+) bulge (Bu) cells in *Egfr*$^{flox/flox}$*K14cre*. (H) Immunofluorescence and quantification of hair follicle stem cells marked by NFATc1 showing reduced NFATc1 (+) hair follicles in *Egfr*$^{flox/flox}$*K14cre* mouse skin sections. (I) Ki67 (proliferation marker) and SOX9 double immunofluorescence and quantification reveals increase in SOX9 (+) bulge cells positive for Ki67 in *Egfr*$^{flox/flox}$*K14cre*. (J) Loss of quiescence as reflected by the colocalization of NFATc1 and Ki67 in *Egfr*$^{flox/flox}$*K14cre*. Arrows denote NFATc1/Ki67 double-positive cells in *Egfr*$^{flox/flox}$*K14cre* bulge. Graphs contain means with SEM ($n \geq 3$ mice; ≥20 hair follicles/mouse). (D, G, I) There were

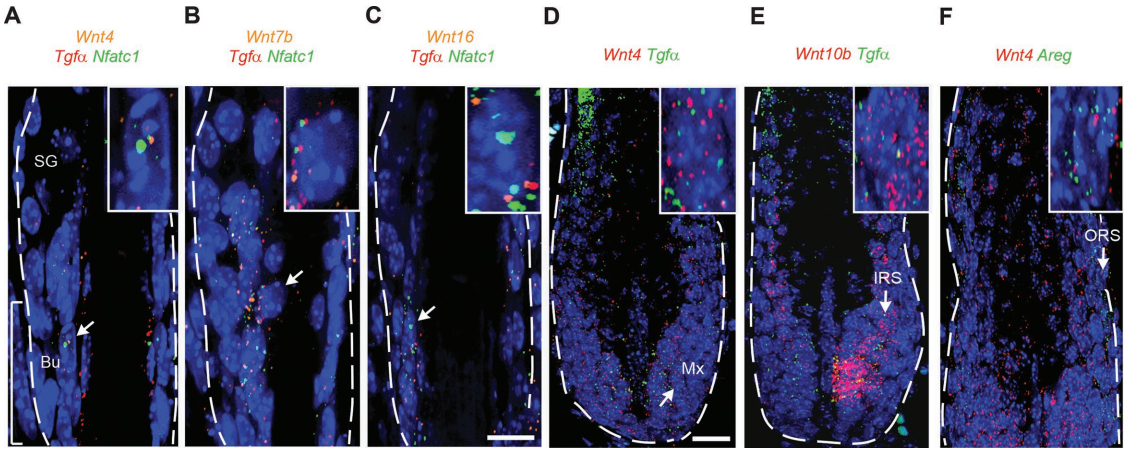

FIGURE 9: Transcripts for EGFR-regulated Wnts and EGFR ligands are colocalized in hair follicle stem cells and their progeny. Multiplex fluorescence ISHs on WT skin sections at P7 detects cellular colocalization of *Tgfα* and *Nfatc1* with *Wnt4* (A), *Wnt7b* (B), or *Wnt16* (C) in bulge (Bu); (D) *Tgfα* with *Wnt4* in matrix (Mx); (E) *Tgfα* with *Wnt10a* in inner root sheath (IRS); and (F) *Areg* with *Wnt4* in outer root sheath (ORS). Arrows denote a nucleus magnified in the inset. Scale bars: 10 μm.

Wnts first appear in the placode and are essential regulators of hair follicle morphogenesis, the hair cycle, and hair follicle stem cell homeostasis (Fu and Hsu, 2013; Myung *et al.*, 2013). Loss of Wnt7b resulted in disruption in hair follicle cycling and hair follicle stem cell maintenance (Kandyba and Kobielak, 2014). Overexpression of Wnt10b induced hair follicle regeneration and promoted follicles to grow larger in size with enhanced proliferation in matrix, dermal papilla, hair shaft, and CD34-positive stem cells (Li *et al.*, 2013). Despite these studies, the factors that regulate Wnt production in the hair follicle during development remain unclear. Our qPCR analyses initially revealed increased mRNAs for multiple *Wnt* genes and β-catenin/TCF target genes in KI skin. Further, using ISH, we demonstrated that loss of EGFR kinase in mice resulted in the up-regulation of *Wnt4*, *6*, *7b*, *10a*, *10b*, and *16* transcripts in epithelial cells of various hair follicle compartments and increases in *Wnt4* and *6* in fibroblasts in the dermal papilla. The concerted nature of the EGFR-mediated negative regulation of *Wnt4*, *6*, *7b*, *10a*, *10b*, and *16* in the hair follicle is very likely to be important during hair follicle development, because Wnts, when expressed in combinations, can act synergistically to stimulate β-catenin signaling (Alok *et al.*, 2017).

Relatively little is currently known about the mechanisms that regulate *Wnt* gene expression. In vitro experiments such as TGFα stimulations of primary mouse keratinocytes and metabolic labeling of newly synthesized RNA with 4sU in keratinocytes treated with TGFα directly linked ligand-induced activation of the EGFR to the inhibition of nascent mRNA synthesis for multiple *Wnt* genes. Additionally, we also demonstrated that EGFR signals through Ras to exert its effect on *Wnt* mRNA levels. Our overall results provide the first mechanistic evidence to show that EGFR can regulate Wnt/β-catenin signaling by repressing the transcription rate of multiple *Wnt* genes.

Studies have shown that the presence and function of hair follicle stem cells directly contribute to hair growth and regeneration, and their absence results in hair loss (Blanpain and Fuchs, 2006). Although EGFR regulates intestinal and neural stem cell proliferation and maintenance (Wong *et al.*, 2012), its role in hair follicle stem cells remains unexplored. Maintenance and quiescence of hair follicle stem cells in the bulge has so far been attributed to control by a combination of extracellular signals (e.g., Wnts, Fgfs, Shh, and Bmp) and expression of transcription factors (e.g., Sox9, Nfatc1, Lhx2, and Tcf3) (Blanpain and Fuchs, 2006; Watt and Jensen, 2009; Tadeu and Horsley, 2014). However, signaling mechanisms that control hair follicle stem cell quiescence, proliferation, and survival during postnatal morphogenesis are not well understood. In our work, we show that EGFR and its ligands are expressed in bulge hair follicle stem cells, and loss of EGFR resulted in unrestrained proliferation in hair follicle stem cells marked with either SOX9 or NFATc1. These hair follicle stem cell populations eventually became exhausted, presumably due to replicative stress. We believe that the reduced number of SOX9-positive cells contributes to the hair follicle defects in EGFR-null mice, because SOX9-positive cells are required to maintain the pool of transit-amplifying cells in the matrix that are necessary to complete hair morphogenesis (Vidal *et al.*, 2005; Nowak *et al.*, 2008). Although NFATc1-expressing quiescent hair follicle stem cells are established during morphogenesis, loss-of-function studies indicate that NFTAc1-positive cells are required for hair cycling but not for postnatal hair morphogenesis (Horsley *et al.*, 2008). Therefore, loss of NFATc1, as in the case of hair follicles lacking EGFR, probably does not impact postnatal hair growth, but signifies an EGFR requirement for maintaining quiescence in stem cells. We also provide strong evidence that elevated levels of *Wnt* transcripts and hyperactivation of the β-catenin pathway in hair follicle stem cells are responsible for stem cell defects in EGFR-null hair follicles. This interpretation of our results is consistent with previously published data demonstrating that elevated

30–75 cells counted per hair follicle. **p* value ≤ 0.05. (K) Increased nuclear β-catenin in *Egfr*$^{flox/flox}$*K14cre* hair follicle matrix (Mx), dermal papilla (DP), and bulge (Bu). Arrow denotes nuclear β-catenin staining in *Egfr*$^{flox/flox}$*K14cre* bulge. (L) Chromogenic ISHs demonstrate up-regulation of *Wnt4* mRNA (red spots) in *Egfr*$^{flox/flox}$*K14cre* matrix, DP, and bulge. (M) Increased *Wnt10b* transcript was observed only in *Egfr*$^{flox/flox}$*K14cre* matrix. Scale bars: 10 μm.

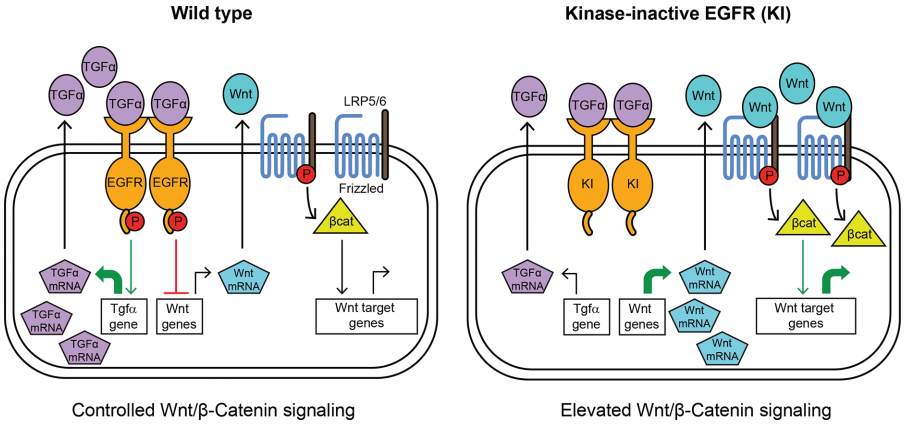

FIGURE 10: EGFR autocrine loops control Wnt signaling. Model of hair follicle cell is presented in which TGFα/EGFR autocrine loop restrains Wnt expression and signaling. In the absence of EGFR kinase (KI), the transcription of *Wnt* genes increases and drives elevated Wnt/β-catenin signaling (right).

Wnt/β-catenin signaling during postnatal hair morphogenesis causes progressive hair loss and depletion of hair follicle stem cells (Huelsken *et al.*, 2001; Narhi *et al.*, 2008; Choi *et al.*, 2013). Together, our data demonstrate that EGFR-mediated attenuation of Wnt/β-catenin signaling is required to control hair follicle stem cell quiescence and rate of proliferation.

On the basis of the totality of our results, we propose a model for how EGFR and Wnt/β-catenin signaling pathways are integrated in cells during hair follicle development, and how loss of EGFR kinase results in elevation of β-catenin signaling (Figure 10). In WT cells, activated EGFR promotes EGFR ligand expression (Figure 10, shown as TGFα) but represses transcription of *Wnt* genes and mRNA levels. EGFR-TGFα autocrine loops are formed and limit Wnt production and signaling (Figure 10, left). The Wnt released from these cells may act in an autocrine manner on the same cell that produces it (Figure 10, shown on the left) or on another cell type in a paracrine manner. In cells that lack EGFR kinase (KI), EGFR-TGFα autocrine loops do not form, transcription of *Wnt* genes rises, and Wnt production is increased. This results in uncontrolled, exaggerated Wnt/β-catenin signaling in the Wnt-releasing KI cells themselves (Figure 10, shown on the right) or in nearby cells. This aberrant Wnt signaling results in increased proliferation, apoptosis, impaired differentiation, and loss of stem cells during hair follicle development.

The EGFR and Wnt/β-catenin signaling pathways are evolutionarily conserved across a wide range of species and are well studied individually within the context of various developmental processes and diseases and as therapeutic targets (Holbro and Hynes, 2004; Logan and Nusse, 2004; Hu and Li, 2010). The mechanism of antagonism between the EGFR and β-catenin signaling pathways that we have observed in the work presented here is distinct from that previously reported in lower organisms (Szuts *et al.*, 1997; Yu *et al.*, 2009). The concept that β-catenin activation lies downstream of EGFR signaling and is responsible for some EGFR-mediated outcomes is intriguing. It is possible that the EGFR–Wnt/β–catenin mechanism we have discovered in the hair follicle is functioning in other biological systems. In general, our findings have many implications and raise several questions. Does EGFR use a similar mechanism to control Wnt/β-catenin signaling during development or homeostasis of other tissues and organs? Is this mechanism operative in diseased states such as cancer? Does EGFR regulate the quiescence or maintenance of other types of stem cells? Does the integration of the EGFR and Wnt/β-catenin pathways influence response or resistance to EGFR-targeted therapies? These important questions merit further investigation.

MATERIALS AND METHODS

Generation of mice that lack EGFR kinase

For generation of KI EGFR mice (KI), a 3.9-kb short-arm DNA fragment was produced by PCR using EGFAT1 and EGFAT2 primers. The EGFAT1 site is located 4.4 kb upstream of exon 19 with a primer sequence of 5′-GTTAGACTTGACCTTGGTGAGATGG-3′, and EGFAT2 is located 0.5 kb upstream of exon 19 with a primer sequence of 5′-ATGCATGAAATTGCATGAGGTCCTACCCT AG-3′ and contains an additional *NsiI* site. The short arm was inserted into the 3′ of the Neo gene cassette flanked by loxP sites using the *NsiI* site. The mid-arm including the mutation within exon 19 was created by a PCR product using the primer pair EGFMA1 and EGFMA2. First, PCR was performed using the primer pair EGFMA1 and EGFMA4 and the primer pair EGFMA3 and EGFMA2. Primer EGFMA1 is located downstream and next to primer EGFAT2 with a sequence of 5′-CCCCTTTCTGCCTTAGCATGTC-3′, and primer EGFMA4 is located inside exon 19 with a sequence of 5′-CTCTTAACTCCATGATGGCCACC-3′ (introduced point mutation underlined). Primer EGFMA2 is located 500 base pairs downstream of exon 19, with a sequence of 5′-CCTGAAGTATGGGCACATCCCTC-3′. Primer EGFMA3, located inside exon 19, has an overlapping sequence with EGFMA4 and the introduced point mutation (underlined) 5′-GGTGGCCATCATGGAGTTAAGAG-3′. The amplified DNA from the PCR products of the two sets of primers was added to the PCR reaction of primer pair EGFMA1 and EGFMA2 to create the final mid-arm. The long arm was an 8-kb genomic fragment consisting of sequence spanning from 0.5 kb upstream to 9.5 kb downstream of exon 19. The targeting vector was linearized and transfected by electroporation of 129/SvEv (iTL1) embryonic stem cells. After selection in G418, surviving colonies were expanded for Southern analysis to identify recombinant clones, and the induced mutation was confirmed by DNA sequencing. Positive clones were injected into C57BL/6J blastocysts to generate chimeric mice, followed by mating to C57BL/6J to obtain heterozygous mutant *Egfr* mice. Genomic sequencing was performed to confirm the targeting event. The neomycin resistance cassette was excised by crossing with an *EIIa-Cre* mouse (Jackson Labs, Bar Harbor, ME), and male mutant mice were backcrossed to Swiss Webster Black (SWB) females for four generations to generate the KI mice used for this study. Genotyping of KI mice was performed by PCR using primers 5′-CAGTTTTCCAGAGGAGGTGGC-3′ and 5′-CACAAATAAGGGGGCTCATCTC-3′, and produced WT and KI allele products of 229 and 350 base pairs, respectively.

Egfr$^{flox/flox}$ (Lee and Threadgill, 2009) and Keratin 14 (*K14*)-Cre (Dassule *et al.*, 2000) mice were obtained from Jackson Labs to create skin-targeted EGFR knockout mice. Hemizygous *K14-Cre* mice were mated with homozygous *Egfr*$^{flox/flox}$ (C57BL/6) mice to obtain *Egfr*$^{flox/+}$;*K14cre* (F1), which were bred subsequently with homozygous *Egfr*$^{flox/flox}$ to generate *Egfr*$^{flox/flox}$; *K14cre* at a 25% Mendelian frequency. Genotyping was performed as described previously (Dassule *et al.*, 2000; Lee and Threadgill, 2009). All animals were maintained and handled according to National Institutes of Health and American Association of Laboratory Animal Care guidelines.

Hair follicle–length measurements

Hair follicle length was quantified using AV Rel 4.8.2 software by measuring the linear distance along an in-plane follicle from the bottom of the leading edge/matrix to the epidermis in the H&E-stained P7 skin sections from WT, KI, and various adenovirus-treated mice.

Histology, immunofluorescence, and imaging

Dorsal skin was dissected and fixed in 4% paraformaldehyde for 24 h at 4°C. Fixed skin samples were dehydrated in an ascending series of alcohol, embedded in paraffin, and sectioned at 5 µm. For histological analysis, H&E staining was performed using standard histological techniques. For immunofluorescence, 5-µm paraffin sections were rehydrated and subjected to antigen retrieval with rodent decloaker (cat. no. RD913L; Biocare Medical) using Retriever 2100 (Electron Microscopy Sciences) for 20 min. Sections were blocked for 15 min in Rodent Block M (for mouse primary antibodies) or Background Punisher (cat. nos. RBM961 and BP974; Biocare Medical). Sections were incubated overnight at 4°C with primary antibodies diluted in Da Vinci Green antibody diluent (cat. no. PD900; Biocare Medical). After three washes with phosphate buffer saline–Tween 20 (PBST) for 15 min at room temperature (RT), sections were incubated with Alexa Fluor–coupled secondary antibodies at a concentration of 1:200 for 1 h at RT. Sections were washed three times in PBST and mounted with ProLong Gold antifade reagent with 4′,6-diamidino-2-phenylindole (cat. no. P36931; ThermoFisher Scientific). Imaging was performed on a Zeiss Upright LSM 710 laser-scanning confocal microscope, and images were captured using Zen software. Figures were prepared using Adobe Photoshop CS4 and Adobe Illustrator. All immunofluorescence analyses were performed on at least three mice per genotype.

Primary mouse keratinocyte cultures and lentiviral transduction

Primary keratinocytes were prepared as previously described (Weinberg *et al.*, 1994). Briefly, keratinocytes were isolated from skin of 1- to 3-d-old mice, pooled, and maintained in Ca^{2+}-free minimal essential medium supplemented with 8% chelexed fetal bovine serum, 0.05 mM Ca^{2+}, and penicillin/streptomycin. The pSLIK-Neo/TRE Pitt lentiviral vector plasmids encoding V5-tagged Ras and dominant-negative (S17N) Ras and lentivirus were generated as described previously (Fan *et al.*, 2013). Primary keratinocytes were transduced by lentivirus, and the following day, expression was induced overnight with 20 ng/ml doxycycline (cat. no. D9891; Sigma-Aldrich). Cells were serum starved for 4 h and then treated with and without murine EGF (30 ng/ml) (cat. no. 315-09; Peprotech) for 6 h in the presence of doxycycline and processed for mRNA and protein analysis.

Metabolic labeling, isolation, and measurement of nascent mRNA

Newly transcribed mRNA was isolated as previously described (Radle *et al.*, 2013). Briefly, primary keratinocyte cultures from WT SWB mice were cultured in 150-mm dishes until close to confluency. After 4 h of serum starvation in 20 ml of basal media, the cells were incubated with 4sU (cat. no. T4509; Sigma-Aldrich) for 15 min and then treated with and without murine TGFα (30 ng/ml) to various time points. Total RNA was isolated with TRIzol Reagent (cat. no. 15596026; ThermoFisher Scientific), and 4sU-incorporated RNA was thiol-specifically biotinylated. Labeled, newly transcribed RNA was then purified from total RNA using streptavidin-coated beads. Finally, labeled RNA from the beads was recovered by adding dithiothreitol and purified using RNeasy MinElute Cleanup kit (cat. no. 74204; Qiagen). qPCR was used to determine 4sU-labeled transcript levels. Relative transcription rates were determined at a time point within the linear phase of transcription. All transcripts were normalized to the *B2m* housekeeping gene.

Antibodies and Western blotting

The following antibodies and dilutions were used for immunofluorescence staining: AE13 (mouse; cat. no. ab16113; 1:100; Abcam), AE15 (mouse; cat. no. ab58755; 1:100; Abcam), β-catenin (rabbit; cat. no. 8480; 1:500; Cell Signaling Technology), Cleaved caspase-3 (Asp175) (rabbit; cat. no. 9579; 1:100; Cell Signaling Technology), γH2AX (Ser-139) (rabbit; cat. no. 2595; 1:400; Cell Signaling Technology), K1 (rabbit; cat. no. 905601; 1:500; Biolegend), K5 (rabbit; cat. no. 905501; 1:2000; Biolegend), K5 (chicken; cat. no. 905901; 1:500; Biolegend), K10 (rabbit; cat. no. 905404; 1:500; Biolegend), K14 (chicken; cat. no. 906004; 1:500; Biolegend), Ki67 (rabbit; cat. no. ab16667; 1:1000; Abcam), Ki67 (mouse; cat. no. 550609; 1:100; BD-Pharmingen), Lor (rabbit; cat. no. 905101; 1:500; Biolegend), NFATc1 (mouse; cat. no. sc-7294; 1:50; Santa Cruz Biotechnology), PH3 (Ser-10) (rabbit; cat. no. 06-570; 1:200; Millipore), PCAD (rat; cat. no. 13-2000Z; 1:25; Invitrogen), pEGFR (Tyr-1173) (mouse; cat. no. 05-483; 1:200; Millipore), PPARγ (rabbit; cat. no. 2435; 1:800; Cell Signaling Technology), SOX9 (rabbit; cat. no. sc-20095; 1:50; Santa Cruz Biotechnology). Secondary antibodies coupled to Alexa Fluor 488, Alexa Fluor 568, or Alexa Fluor 647 were obtained from Life Technologies. Antibodies used against sFRP1 were previously described (Uren *et al.*, 2000). EGFR (rabbit; cat. no. 06-847; 1:500; Millipore), phospho-p44/42 MAPK (Erk1/2) (Thr-202/Tyr-204) (rabbit; cat. no. 9101; 1:1000; Cell Signaling Technology), V5 (rabbit; cat. no. 13202; 1:1000; Cell Signaling Technology), β-catenin (rabbit; cat. no. 8480; 1:500; Cell Signaling Technology), Lef1 (rabbit; cat. no. 2230; 1:500; Cell Signaling Technology), GFP (chicken; cat. no. ab13970; 1:5000; Abcam) TUBA1A (mouse; cat. no. CP06; 1:1000; Millipore), β-actin (mouse; cat. no. sc-47778; 1:500; Santa Cruz Biotechnology), and GAPDH (mouse; cat. no. GTX627408; 1:1000; GeneTex) were used for Western blotting. Western blotting was performed as previously described (Fan *et al.*, 2013).

In situ hybridization

RNA ISH was carried out using the RNAScope ISH technology (Advanced Cell Diagnostic, Hayward, CA) (Wang *et al.*, 2012). Briefly, dorsal skin was fixed in 10% neutral buffered Formalin for 24 h at RT, dehydrated, and embedded in paraffin. Skin sections were cut at 5-µm thickness, air-dried overnight at RT, and processed for RNA in situ detection using RNAscope 2.5 HD Reagent Kit-RED (cat. no. 322360) for chromogenic detection and RNAscope Fluorescent Multiplex Kit (cat. no. 320850) for fluorescence detection according to the manufacturer's instructions. To ensure RNA integrity and test the assay procedure, we subjected dewaxed and rehydrated skin sections to pretreatment conditions optimized to 10-min heat pretreatment at 95°C, followed by 20-min protease digestion at 40°C. RNAscope probes used were: *Wnt4* (cat. nos. 401101 and 401101-C2), *Wnt6* (cat. no. 401111), *Wnt7b* (cat. no. 401131), *Wnt10a* (cat. no. 401061), *Wnt10b* (cat. no. 401071), *Wnt16* (cat. no. 401081), *Axin2* (cat. no. 400331), *Lef1* (cat. no. 405021), *Lgr6* (cat. no. 404961), *Sox9* (cat. no. 401051-C2), *Nfatc1* (cat. no. 436161-C2 and cat. no.436161-C3), *Tgfα* (cat. nos. 435251 and 435251-C2), *Areg* (cat. nos. 430501 and 430501-C2), *Ereg* (cat. no. 437981), *Btc* (cat. no. 437961), *Hbegf* (cat. no. 437601), *Epgn* (cat. no. 437971), *Egf* (cat. no. 434231), *Egfr* (cat. no. 443551), and *Cd34* (cat. no. 319161). Probes targeting cyclophilin B (*Ppib*) (cat. no. 313911) mRNA and

bacterial mRNA *DapB* (cat. no. 310043) were used as positive and negative controls, respectively, to assess tissue and RNA quality. Multiplex fluorescence ISH-stained hair follicles were imaged using a Zeiss LSM 710 confocal microscope at 40× magnification with Zen software (Carl Zeiss). All microscope and camera settings (light level, exposure, gain, etc.) were identical for all images. Each individual RNA molecule appears as a distinct punctate dot (Wang *et al.*, 2012). For quantification of ISH signals, *Nfatc1*- or *Sox9*-positive cells were first identified, and the transcript levels of *Wnts* and β-catenin target genes were scored by manually counting the number of signal dots in these cells. More than 75 *Nfatc1*$^+$ or *Sox9*$^+$ cells were counted in at least three mice per genotype. The relative transcript level per *Nfatc1*$^+$ or *Sox9*$^+$ cell is calculated by the number of *Wnt* and β-catenin target gene mRNAs (dots) in *Nfatc1*$^+$ or *Sox9*$^+$ cells divided by the total number of *Nfatc1*- or *Sox9*-labeled cells.

RNA extraction and qPCR

Total RNA was prepared using the RNeasy plus micro kit (cat. no. 74034; Qiagen) according to the manufacturer's recommendations. Purified RNA was used to synthesize the first-strand cDNA using Superscript VILO master mix (cat. no. 11755050; ThermoFisher Scientific). qPCR was performed on a QuantStudio 7 Flex System using a TaqMan universal PCR master mix (cat. no. 4304437; ThermoFisher Scientific) to measure *Wnt3*, *Wnt3a*, *Wnt4*, *Wnt5a*, *Wnt5b*, *Wnt6*, *Wnt7a*, *Wnt7b*, *Wnt10a*, *Wnt10b*, *Wnt11*, *Wnt16*, *Axin2*, *Lef1*, *Lgr6*, *and c-Myc* mRNA. All transcripts were normalized to the housekeeping genes *Gapdh* and *B2M*.

Adenovirus administration

GFP and mouse sFRP1 adenoviruses were from Vector Biolabs. A single subcutaneous injection was made into dorsal skin of mice at P4 along the cephalocaudal axis at a dose of 10^8 plaque formation unit/g body weight. The injection was angled toward the head and produced a 1-cm wheal, which was outlined with permanent marker. Skin in the marked area was harvested at P7 and processed for molecular and histological analyses.

ACKNOWLEDGMENTS

We thank M. Kukuruga and A. D. Akue for fluorescence-activated cell sorting (Food and Drug Administration [FDA]/Center for Biologics Evaluation and Research [CBER] Flow Cytometry Core); Wells Wu for performing RNA-Seq (FDA/CBER Core); Svetlana Petrovskaya, Alin Voskanian-Kordi, and Luis Santana-Quintero for performing RNA-Seq analysis; all personnel in the division of veterinary services for mouse care; and Xinyi Liu for the Figure 10 illustration.

REFERENCES

Alenzi FQ (2004). Links between apoptosis, proliferation and the cell cycle. Br J Biomed Sci 61, 99–102.

Alok A, Lei Z, Jagannathan NS, Kaur S, Harmston N, Rozen SG, Tucker-Kellogg L, Virshup DM (2017). Wnt proteins synergize to activate beta-catenin signaling. J Cell Sci 130, 1532–1544.

Alonso L, Fuchs E (2006). The hair cycle. J Cell Sci 119, 391–393.

Baker CM, Verstuyf A, Jensen KB, Watt FM (2010). Differential sensitivity of epidermal cell subpopulations to beta-catenin-induced ectopic hair follicle formation. Dev Biol 343, 40–50.

Bichsel KJ, Hammiller B, Trempus CS, Li Y, Hansen LA (2016). The epidermal growth factor receptor decreases Stathmin 1 and triggers catagen entry in the mouse. Exp Dermatol 25, 275–281.

Blanpain C, Fuchs E (2006). Epidermal stem cells of the skin. Annu Rev Cell Dev Biol 22, 339–373.

Castilho RM, Squarize CH, Chodosh LA, Williams BO, Gutkind JS (2009). mTOR mediates Wnt-induced epidermal stem cell exhaustion and aging. Cell Stem Cell 5, 279–289.

Cheung TH, Rando TA (2013). Molecular regulation of stem cell quiescence. Nat Rev Mol Cell Biol 14, 329–340.

Choi YS, Zhang Y, Xu M, Yang Y, Ito M, Peng T, Cui Z, Nagy A, Hadjantonakis AK, Lang RA, *et al.* (2013). Distinct functions for Wnt/beta-catenin in hair follicle stem cell proliferation and survival and interfollicular epidermal homeostasis. Cell Stem Cell 13, 720–733.

Dassule HR, Lewis P, Bei M, Maas R, McMahon AP (2000). Sonic hedgehog regulates growth and morphogenesis of the tooth. Development 127, 4775–4785.

Duverger O, Morasso MI (2009). Epidermal patterning and induction of different hair types during mouse embryonic development. Birth Defects Res C Embryo Today 87, 263–272.

Fan YX, Wong L, Marino MP, Ou W, Shen Y, Wu WJ, Wong KK, Reiser J, Johnson GR (2013). Acquired substrate preference for GAB1 protein bestows transforming activity to ERBB2 kinase lung cancer mutants. J Biol Chem 288, 16895–16904.

Fu J, Hsu W (2013). Epidermal Wnt controls hair follicle induction by orchestrating dynamic signaling crosstalk between the epidermis and dermis. J Invest Dermatol 133, 890–898.

Gat U, DasGupta R, Degenstein L, Fuchs E (1998). De Novo hair follicle morphogenesis and hair tumors in mice expressing a truncated beta-catenin in skin. Cell 95, 605–614.

Hansen LA, Alexander N, Hogan ME, Sundberg JP, Dlugosz A, Threadgill DW, Magnuson T, Yuspa SH (1997). Genetically null mice reveal a central role for epidermal growth factor receptor in the differentiation of the hair follicle and normal hair development. Am J Pathol 150, 1959–1975.

Holbro T, Hynes NE (2004). ErbB receptors: directing key signaling networks throughout life. Annu Rev Pharmacol Toxicol 44, 195–217.

Horsley V, Aliprantis AO, Polak L, Glimcher LH, Fuchs E (2008). NFATc1 balances quiescence and proliferation of skin stem cells. Cell 132, 299–310.

Hu T, Li C (2010). Convergence between Wnt-beta-catenin and EGFR signaling in cancer. Mol Cancer 9, 236.

Huelsken J, Vogel R, Erdmann B, Cotsarelis G, Birchmeier W (2001). Beta-Catenin controls hair follicle morphogenesis and stem cell differentiation in the skin. Cell 105, 533–545.

Huse M, Kuriyan J (2002). The conformational plasticity of protein kinases. Cell 109, 275–282.

Kadaja M, Keyes BE, Lin M, Pasolli HA, Genander M, Polak L, Stokes N, Zheng D, Fuchs E (2014). SOX9: a stem cell transcriptional regulator of secreted niche signaling factors. Genes Dev 28, 328–341.

Kandyba E, Kobielak K (2014). Wnt7b is an important intrinsic regulator of hair follicle stem cell homeostasis and hair follicle cycling. Stem Cells 32, 886–901.

Kandyba E, Leung Y, Chen YB, Widelitz R, Chuong CM, Kobielak K (2013). Competitive balance of intrabulge BMP/Wnt signaling reveals a robust gene network ruling stem cell homeostasis and cyclic activation. Proc Natl Acad Sci USA 110, 1351–1356.

Kern F, Niault T, Baccarini M (2011). Ras and Raf pathways in epidermis development and carcinogenesis. Br J Cancer 104, 229–234.

Lee TC, Threadgill DW (2009). Generation and validation of mice carrying a conditional allele of the epidermal growth factor receptor. Genesis 47, 85–92.

Li YH, Zhang K, Yang K, Ye JX, Xing YZ, Guo HY, Deng F, Lian XH, Yang T (2013). Adenovirus-mediated Wnt10b overexpression induces hair follicle regeneration. J Invest Dermatol 133, 42–48.

Lichtenberger BM, Gerber PA, Holcmann M, Buhren BA, Amberg N, Smolle V, Schrumpf H, Boelke E, Ansari P, Mackenzie C, *et al.* (2013). Epidermal EGFR controls cutaneous host defense and prevents inflammation. Sci Transl Med 5, 199ra111.

Lien WH, Polak L, Lin M, Lay K, Zheng D, Fuchs E (2014). In vivo transcriptional governance of hair follicle stem cells by canonical Wnt regulators. Nat Cell Biol 16, 179–190.

Lim X, Nusse R (2013). Wnt signaling in skin development, homeostasis, and disease. Cold Spring Harb Perspect Biol 5, a008029.

Lim X, Tan SH, Yu KL, Lim SB, Nusse R (2016). Axin2 marks quiescent hair follicle bulge stem cells that are maintained by autocrine Wnt/beta-catenin signaling. Proc Natl Acad Sci USA 113, E1498–E1505.

Lo Celso C, Prowse DM, Watt FM (2004). Transient activation of beta-catenin signalling in adult mouse epidermis is sufficient to induce new hair follicles but continuous activation is required to maintain hair follicle tumours. Development 131, 1787–1799.

Logan CY, Nusse R (2004). The Wnt signaling pathway in development and disease. Annu Rev Cell Dev Biol 20, 781–810.

Lowry WE, Blanpain C, Nowak JA, Guasch G, Lewis L, Fuchs E (2005). Defining the impact of beta-catenin/Tcf transactivation on epithelial stem cells. Genes Dev 19, 1596–1611.

Lynch MH, O'Guin WM, Hardy C, Mak L, Sun TT (1986). Acidic and basic hair/nail ("hard") keratins: their colocalization in upper cortical and

cuticle cells of the human hair follicle and their relationship to "soft" keratins. J Cell Biol 103, 2593–2606.
Mah LJ, El-Osta A, Karagiannis TC (2010). GammaH2AX: a sensitive molecular marker of DNA damage and repair. Leukemia 24, 679–686.
Mascia F, Lam G, Keith C, Garber C, Steinberg SM, Kohn E, Yuspa SH (2013). Genetic ablation of epidermal EGFR reveals the dynamic origin of adverse effects of anti-EGFR therapy. Sci Transl Med 5, 199ra110.
Miettinen PJ, Berger JE, Meneses J, Phung Y, Pedersen RA, Werb Z, Derynck R (1995). Epithelial immaturity and multiorgan failure in mice lacking epidermal growth factor receptor. Nature 376, 337–341.
Mikels AJ, Nusse R (2006). Wnts as ligands: processing, secretion and reception. Oncogene 25, 7461–7468.
Millar SE (2002). Molecular mechanisms regulating hair follicle development. J Invest Dermatol 118, 216–225.
Muller-Rover S, Handjiski B, van der Veen C, Eichmuller S, Foitzik K, McKay IA, Stenn KS, Paus R (2001). A comprehensive guide for the accurate classification of murine hair follicles in distinct hair cycle stages. J Invest Dermatol 117, 3–15.
Myung PS, Takeo M, Ito M, Atit RP (2013). Epithelial Wnt ligand secretion is required for adult hair follicle growth and regeneration. J Invest Dermatol 133, 31–41.
Nanba D, Toki F, Barrandon Y, Higashiyama S (2013). Recent advances in the epidermal growth factor receptor/ligand system biology on skin homeostasis and keratinocyte stem cell regulation. J Dermatol Sci 72, 81–86.
Narhi K, Jarvinen E, Birchmeier W, Taketo MM, Mikkola ML, Thesleff I (2008). Sustained epithelial beta-catenin activity induces precocious hair development but disrupts hair follicle down-growth and hair shaft formation. Development 135, 1019–1028.
Nowak JA, Polak L, Pasolli HA, Fuchs E (2008). Hair follicle stem cells are specified and function in early skin morphogenesis. Cell Stem Cell 3, 33–43.
O'Guin WM, Sun TT, Manabe M (1992). Interaction of trichohyalin with intermediate filaments: three immunologically defined stages of trichohyalin maturation. J Invest Dermatol 98, 24–32.
Radle B, Rutkowski AJ, Ruzsics Z, Friedel CC, Koszinowski UH, Dolken L (2013). Metabolic labeling of newly transcribed RNA for high resolution gene expression profiling of RNA synthesis, processing and decay in cell culture. J Vis Exp 78, 50195.
Red Brewer M, Choi SH, Alvarado D, Moravcevic K, Pozzi A, Lemmon MA, Carpenter G (2009). The juxtamembrane region of the EGF receptor functions as an activation domain. Mol Cell 34, 641–651.
Reddy S, Andl T, Bagasra A, Lu MM, Epstein DJ, Morrisey EE, Millar SE (2001). Characterization of Wnt gene expression in developing and postnatal hair follicles and identification of Wnt5a as a target of Sonic hedgehog in hair follicle morphogenesis. Mech Dev 107, 69–82.
Scaltriti M, Baselga J (2006). The epidermal growth factor receptor pathway: a model for targeted therapy. Clin Cancer Res 12, 5268–5272.
Schmidt-Ullrich R, Paus R (2005). Molecular principles of hair follicle induction and morphogenesis. BioEssays 27, 247–261.
Schneider MR, Schmidt-Ullrich R, Paus R (2009). The hair follicle as a dynamic miniorgan. Curr Biol 19, R132–R142.
Sennett R, Rendl M (2012). Mesenchymal-epithelial interactions during hair follicle morphogenesis and cycling. Semin Cell Dev Biol 23, 917–927.
Sibilia M, Wagner EF (1995). Strain-dependent epithelial defects in mice lacking the EGF receptor. Science 269, 234–238.
Szuts D, Freeman M, Bienz M (1997). Antagonism between EGFR and Wingless signalling in the larval cuticle of *Drosophila*. Development 124, 3209–3219.
Tadeu AM, Horsley V (2014). Epithelial stem cells in adult skin. Curr Top Dev Biol 107, 109–131.
Threadgill DW, Dlugosz AA, Hansen LA, Tennenbaum T, Lichti U, Yee D, LaMantia C, Mourton T, Herrup K, Harris RC, *et al*. (1995). Targeted disruption of mouse EGF receptor: effect of genetic background on mutant phenotype. Science 269, 230–234.
Uren A, Reichsman F, Anest V, Taylor WG, Muraiso K, Bottaro DP, Cumberledge S, Rubin JS (2000). Secreted frizzled-related protein-1 binds directly to Wingless and is a biphasic modulator of Wnt signaling. J Biol Chem 275, 4374–4382.
Vasioukhin V, Degenstein L, Wise B, Fuchs E (1999). The magical touch: genome targeting in epidermal stem cells induced by tamoxifen application to mouse skin. Proc Natl Acad Sci USA 96, 8551–8556.
Vidal VP, Chaboissier MC, Lutzkendorf S, Cotsarelis G, Mill P, Hui CC, Ortonne N, Ortonne JP, Schedl A (2005). Sox9 is essential for outer root sheath differentiation and the formation of the hair stem cell compartment. Curr Biol 15, 1340–1351.
Wang F, Flanagan J, Su N, Wang LC, Bui S, Nielson A, Wu X, Vo HT, Ma XJ, Luo Y (2012). RNAscope: a novel in situ RNA analysis platform for formalin-fixed, paraffin-embedded tissues. J Mol Diagn 14, 22–29.
Watt FM, Jensen KB (2009). Epidermal stem cell diversity and quiescence. EMBO Mol Med 1, 260–267.
Weinberg WC, Azzoli CG, Kadiwar N, Yuspa SH (1994). p53 gene dosage modifies growth and malignant progression of keratinocytes expressing the v-rasHa oncogene. Cancer Res 54, 5584–5592.
Wieduwilt MJ, Moasser MM (2008). The epidermal growth factor receptor family: biology driving targeted therapeutics. Cell Mol Life Sci 65, 1566–1584.
Wong VW, Stange DE, Page ME, Buczacki S, Wabik A, Itami S, van de Wetering M, Poulsom R, Wright NA, Trotter MW, *et al*. (2012). Lrig1 controls intestinal stem-cell homeostasis by negative regulation of ErbB signalling. Nat Cell Biol 14, 401–408.
Yi R (2017). Concise review: mechanisms of quiescent hair follicle stem cell regulation. Stem Cells 35, 2323–2330.
Yu H, Seah A, Herman MA, Ferguson EL, Horvitz HR, Sternberg PW (2009). Wnt and EGF pathways act together to induce *C.elegans* male hook development. Dev Biol 327, 419–432.
Zhu X, Wu Y, Huang S, Chen Y, Tao Y, Wang Y, He S, Shen S, Wu J, Guo X, *et al*. (2014). Overexpression of Wnt5a in mouse epidermis causes no psoriasis phenotype but an impairment of hair follicle anagen development. Exp Dermatol 23, 926–928.